Cold-Inducible RNA-binding protein (CIRBP) adjusts clock gene expression and REM sleep recovery following sleep deprivation

Marieke MB Hoekstra, Yann Emmenegger, Paul Franken

Center for Integrative Genomics, University of Lausanne, Lausanne, Switzerland

Corresponding author: paul.franken@unil.ch

Short title: *Cirbp* adjusts SD-induced changes in clock gene expression

Abstract

Sleep depriving mice affects clock gene expression, suggesting that these genes partake in sleep homeostasis. The mechanisms linking wakefulness to clock gene expression are, however, not well understood. We propose CIRBP because its rhythmic expression is i) sleep-wake driven and ii) necessary for high-amplitude clock gene expression *in vitro*. We therefore expect *Cirbp* knock-out (KO) mice to exhibit attenuated sleep-deprivation (SD) induced changes in clock gene expression, and consequently to differ in their sleep homeostatic regulation. Lack of CIRBP indeed blunted the SD-incurred changes in cortical expression of the clock gene *Rev-erbα* whereas it amplified the changes in *Per2* and *Clock*. Concerning sleep homeostasis, KO mice accrued only half the extra REM sleep wild-type (WT) littermates obtained during recovery. Unexpectedly, KO mice were more active during lights-off which was accompanied by an acceleration of theta oscillations. Thus, CIRBP adjusts cortical clock gene expression after SD and expedites REM sleep recovery.

Keywords: mice, sleep, *Cirbp*, cortical temperature, clock genes, locomotor activity, REM sleep, circadian rhythms

Introduction

The sleep-wake distribution is coordinated by the interaction of a circadian and a sleep homeostatic process (Daan et al., 1984). The molecular basis of the circadian process consists of clock genes that interact through transcriptional/translational feedback loops. CLOCK/NPAS2:BMAL1 heterodimers drive the transcription of many target genes, among which *Period* (*Per1-2*), *Cryptochome* (*Cry1*, *-2*), and *Rev-Erb (Nr1d1, -2)*. Subsequently, PER:CRY complexes inhibit CLOCK/NPAS2:BMAL1 transcriptional activity and thus prevent their own transcription. Through another loop, other clock components such as the transcriptional repressor REV-ERBα regulate the transcription of *Bmal1* (*Arntl*), ensuring together with other transcriptional feedback loops a period of ca. 24 hours (Lowrey and Takahashi, 2011).

The sleep homeostatic process keeps track of time spent awake and time spent asleep, during which sleep pressure is increasing and decreasing, respectively. The mechanisms underlying this process are to date unknown. However, accumulating evidence implicates clock genes in sleep homeostasis [reviewed in (Franken, 2013)]. This is supported by studies in several species (*i.e.* mice, fruit flies and humans), showing that mutations in circadian clock genes are associated with an

49 altered sleep homeostatic response to sleep deprivation (SD) [*e.g.* (Mang et al., 2016, Shaw et al.,
50 2002, Viola et al., 2007, Wisor et al., 2002)]. Furthermore, SD affects the expression of clock genes
51 such as *Rev-erbα*, *Per1-3* and *Dbp* (Mongrain et al., 2010), but the mechanisms through which this
52 occurs are unclear.

53 In this study, we examined one such mechanism and hypothesized that some of the SD-induced
54 changes in clock gene expression occur through Cold-Inducible RNA Binding Protein (CIRBP).
55 Decreasing temperature *in vitro* increases CIRBP levels (Nishiyama et al., 1997) and the daily
56 changes in body temperature of the mouse are sufficient to drive robust cyclic levels of *Cirbp* and
57 CIRBP (Morf et al., 2012) in anti-phase with temperature. Although the daily changes in cortical
58 temperature (T_{cx}) appear circadian, more than 80% of its variance is explained by the sleep-wake
59 distribution in the rat (Franken et al., 1992). Hence, the daily rhythms of cortical *Cirbp* become
60 strongly attenuated when controlling for these sleep-wake driven changes in T_{cx} by SDs (see Figure
61 1, based on Gene Expression Omnibus number GSE9442 from Maret et al., 2007). Furthermore,
62 *Cirbp* is the top down-regulated gene after SD (Mongrain et al., 2010, Wang et al., 2010)
63 underscoring again its sleep-wake dependent expression. But how does CIRBP relate to clock gene
64 expression?

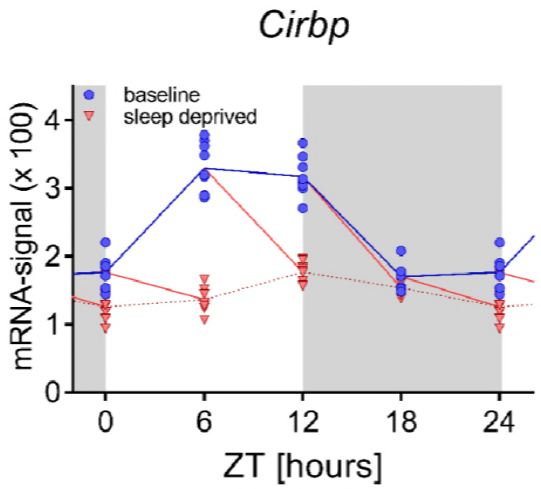

Figure 1 **The sleep-wake distribution drives daily changes of central *Cirbp* expression in the mouse**. After the onset of the baseline rest phase (ZT0), when mice spend more time asleep and thus T_{cx} decreases, *Cirbp* expression increases (blue symbols and lines), whereas between ZT12-18, when mice spent most of their time awake and T_{cx} is high, *Cirbp* decreases. When controlling for these diurnal changes in sleep-wake distribution by performing four 6h SD [sleep deprivation] starting at either ZT0, -6, -12, or -18, the diurnal amplitude of *Cirbp* is greatly reduced (red symbols represent levels of expression reached at the end of the SD). Nine biological replicates per time point and condition from three different inbred strains of mice were used (one data point missing at ZT18), and RNA was extracted from whole brain tissue (see Maret et al. 2007 for details). Data were taken from GEO GSE9442 and accessible in source file 1.

65

66 Two independent studies showed that the temperature-driven changes in CIRBP are required
67 for high amplitude clock gene expression in temperature synchronized cells (Morf et al., 2012, Liu
68 et al., 2013). Therefore, we and others (Archer et al., 2014) hypothesized that changes in clock gene
69 expression during SD are a consequence of the sleep-wake driven changes in CIRBP. We used mice

70 lacking CIRBP (*Cirbp* KO) (Masuda et al., 2012) to test this hypothesis. We first assessed whether
71 also in the mouse the daily changes in T_{cx} are driven by the sleep-wake distribution and what the
72 contribution of locomotor activity (LMA) to these changes was. Next, we assessed SD-induced
73 changes in clock gene expression in WT and KO mice. Because we expected that the response to
74 SD in terms of clock gene expression differed in KO mice, and clock genes partake in sleep
75 homeostasis (Franken, 2013), we also assessed the homeostatic regulation of sleep in *Cirbp* KO and
76 WT mice.

77 Our experiments revealed that also in the mouse the sleep-wake distribution is the major
78 determinant of changes in T_{cx}, with a significant albeit small contribution of LMA. In line with our
79 predictions, we found that lack of CIRBP indeed attenuated the SD-induced changes in the cortical
80 expression of *Rev-erbα* and the homeostatic response in REM sleep time. However, in contrast to
81 our hypothesis, we observed that the changes in *Per2* and *Clock* expression after SD were
82 augmented in *Cirbp* KO mice. Unexpectedly, we discovered that *Cirbp* KO mice were substantially
83 more active compared to their WT littermates without increasing their time spent awake. This
84 dark-phase increase in LMA was accompanied by an acceleration of EEG theta oscillations during
85 active waking. Altogether, our data show that *Cirbp* contributes to some of the SD-induced changes
86 in clock gene expression, but also points to the existence of other sleep-wake driven pathways
87 conveying sleep-wake state to clock gene expression.

88

Results

THE RELATION BETWEEN CORTICAL TEMPERATURE (T_{CX}), SLEEP-WAKE DISTRIBUTION, AND LOCOMOTOR ACTIVITY (LMA)

The dependence of brain or cortical temperature on sleep-wake state has been demonstrated in a number of mammals (Alfoldi et al., 1990, Baker and Hayward, 1968, Deboer et al., 1994, Franken et al., 1992, Hayward and Baker, 1968) but has not been specifically addressed in the mouse. Moreover, no study so far specifically controlled for LMA when quantifying the contribution of sleep-wake state to brain temperature. We therefore measured cortical temperature (T_{cx}), LMA and sleep-wake state in WT and *Cirbp* KO mice during two baseline days, a 6hr SD and the following two recovery days. Because the relationship between T_{cx}, LMA, and waking in WT and KO mice was alike, we illustrated the results in WT mice only.

Fast changes in T_{cx} occur at sleep-wake state transitions

A representative example of a 96h recording of LMA, sleep-wake state and T_{cx} is depicted in Figure 2. Consistent with mice being nocturnal animals, the mouse shows more waking and LMA, and overall higher T_{cx} levels during the dark phase. SD on the third recording day (between Zeitgeber Time (ZT)0-6) led to an almost uninterrupted period of 6hr waking, during which LMA and T_{cx} reached values comparable to bouts of spontaneous wakefulness under undisturbed baseline conditions (*i.e.*, ZT12-18). A closer inspection of the rapid changes in T_{cx} suggests that sleep-wake state transitions underlie these fluctuations. We further quantified these sleep-wake evoked changes in T_{cx} by selecting and aligning transitions between consolidated bouts of NREM and REM sleep and wakefulness during the two baseline days (Figure 2-B). When entering NREM sleep, T_{cx} consistently decreased, whereas at a transition into wake and REM sleep, T_{cx} increased. The latter transition was characterized by a fast and consistent change in T_{cx}; within 1.5 minutes, T_{cx} increased by 0.4°C. The subsequent transition from REM sleep into wake leads to an initial decrease in T_{cx} and contrasts with the waking-evoked increase in T_{cx} when transitioning from NREM sleep to wake. Altogether, these results provide evidence that sleep-wake state importantly contributes to changes in T_{cx}. The sleep-wake state evoked changes in T_{cx} did not differ between genotypes (2-way RM ANOVA, factors genotype (GT) and Time; GT: $p>0.13$, GTxTime: $p>0.09$).

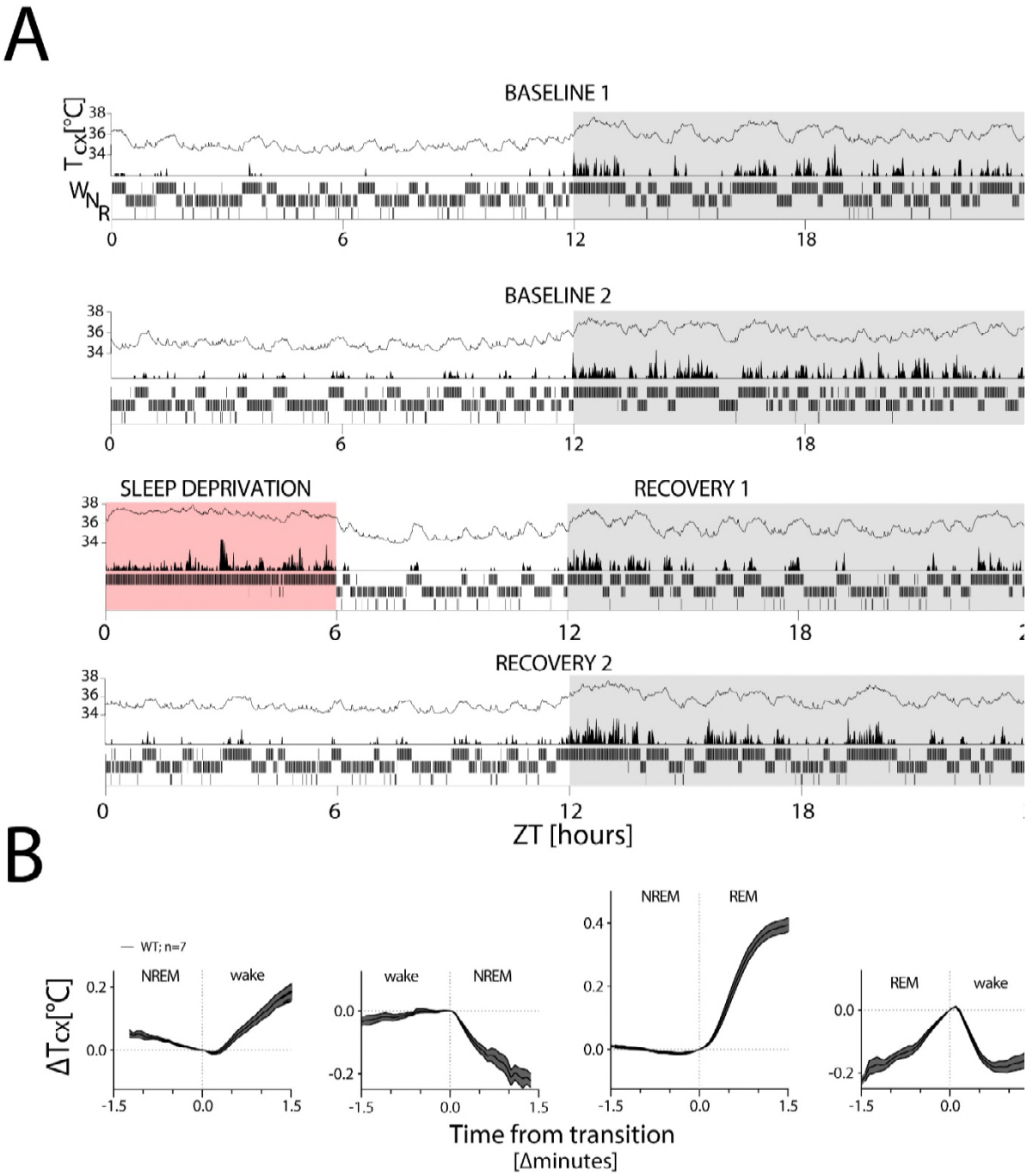

Figure 2 **T_{cx} changes with sleep-wake state.** T_{cx}: cortical temperature; LMA: locomotor activity. **(A)** A representative four-day recording of one mouse in LD 12:12 (in white:grey) during two baseline days (top 2 panels), followed by a 6hr SD (in red; third panel) and two recovery days (bottom 2 panels), with within each panel T_{cx} (top; line graph), LMA (middle; area plot) and sleep-wake states (bottom; hypnogram). Sleep-wake states are averaged per minute to aid visualization. LMA was collected and plotted per minute (see Methods). **(B)** changes in T_{cx}, depicted as mean±SEM, relative to T_{cx} at the sleep-wake transition (average of the last value before and first value after transition). T_{cx} increased when transitioning from NREM sleep to wake and to REM sleep (1-way RM ANOVA, factor Time, $F(36,180)=40.8$, $F(44,264)=222$; $p<0.0001$, respectively) and decreased when transitioning from wake to NREM sleep ($F(22,132)=1.8$, $p=0.02$). Also the transition from REM sleep to wake affected the time course of T_{cx} ($F(23,138)=48.9$, $p<0.0001$). Transition data were obtained from both baseline recordings (see Methods for details).

121 *Daily cycles in T_{cx} are determined by sleep-wake state*

122 After having established that the rapid changes in T_{cx} are indeed evoked by changes in sleep-
123 wake state, we next wondered if the large daily change in T_{cx} is also due to the daily rhythms in
124 sleep-wake state and LMA, and therefore inspected these variables per hour. The LMA data were
125 $\log_2$ transformed to allow for parametric assessment. T_{cx}, waking and LMA oscillated over the course
126 of the 24h baseline (BL) in similar fashion in both genotypes (2-way RM ANOVA on BL1 and -2
127 averaged 1h intervals, Factor Time: $F(23,207)=70.5$; 27.2; 22.5; $p<0.0001$, respectively, Figure 3-A,
128 Factor GT x Time (1,24); T_{cx}: $F(23,207)=0.9$, $p=0.63$; waking: 1.7, $p=0.03$, LMA: 1.21, $p=0.24$) and the
129 amplitude of the BL change in T_{cx} did not differ between genotypes (WT: 2.34±0.1, KO: 2.33±0.1; t-
130 test: $t(9)=-0.02$, $p=0.98$; average of the difference between the highest and lowest value hourly value
131 in BL1 and -2). Importantly, the time course of waking and LMA both closely resembled that of T_{cx}.
132 This observation was supported by the strong correlation between T_{cx} and waking (Figure 3-B left:
133 WT: $R^2=0.76$; KO: $R^2=0.81$, $p<0.0001$) and between T_{cx} and LMA (Figure 3-B right: WT: $R^2=0.60$; KO:
134 $R^2=0.72$, $p<0.0001$).

135 To assess the influence of waking on T_{cx} at a time of day when T_{cx} is normally low and mice
136 spend most of their time asleep, mice were sleep deprived between ZT0 and ZT6. Mice were 98%
137 of the 6hr SD awake, and thus more awake and active compared to the same time under BL
138 conditions (paired t-test: waking [hours] BL: 2.2±0.1, SD: 5.9±0.04; $t(10)=-38.1$, $p<0.0001$;
139 $\log_2$[movements], BL: 13.1±2.4, SD: 39.4±2.1; $t(10)=-15.2$, $p<0.0001$). These changes led to sustained
140 elevated T_{cx} (average ZT0-ZT6 [°C]: BL: 34.7±0.07, SD: 36.6±0.06, $t(10)=-44.3$, $p<0.0001$), suggesting
141 that wakefulness and/or LMA drives changes in T_{cx}. Genotype did not contribute to or interact with
142 these changes (2-way ANOVA, GT*SD/BL: $p>0.39$)

143 However, factors accompanying the SD other than extended waking, such as stress, could have
144 contributed to the SD-induced changes in T_{cx}. To address this issue, we selected within each mouse
145 the longest uninterrupted spontaneous waking bout occurring during BL (average bout length:
146 100±19 minutes). We then compared T_{cx} during the last 10 minutes of this spontaneous waking bout
147 (to reduce any effects of differences in T_{cx} at bout-onset) with T_{cx} reached in the last 10 minutes of
148 an equivalent time spent awake from the start of the SD on. T_{cx} reached during the SD and
149 spontaneous wakefulness did not differ (Figure 3-C), also not in KO mice ($t(5)=0.84$, $p=0.44$),
150 indicating that factors other than extended wakefulness (*e.g.* light exposure, circadian time, SD-
151 associated stress) do not importantly contribute to the changes in T_{cx} during the SD.

152

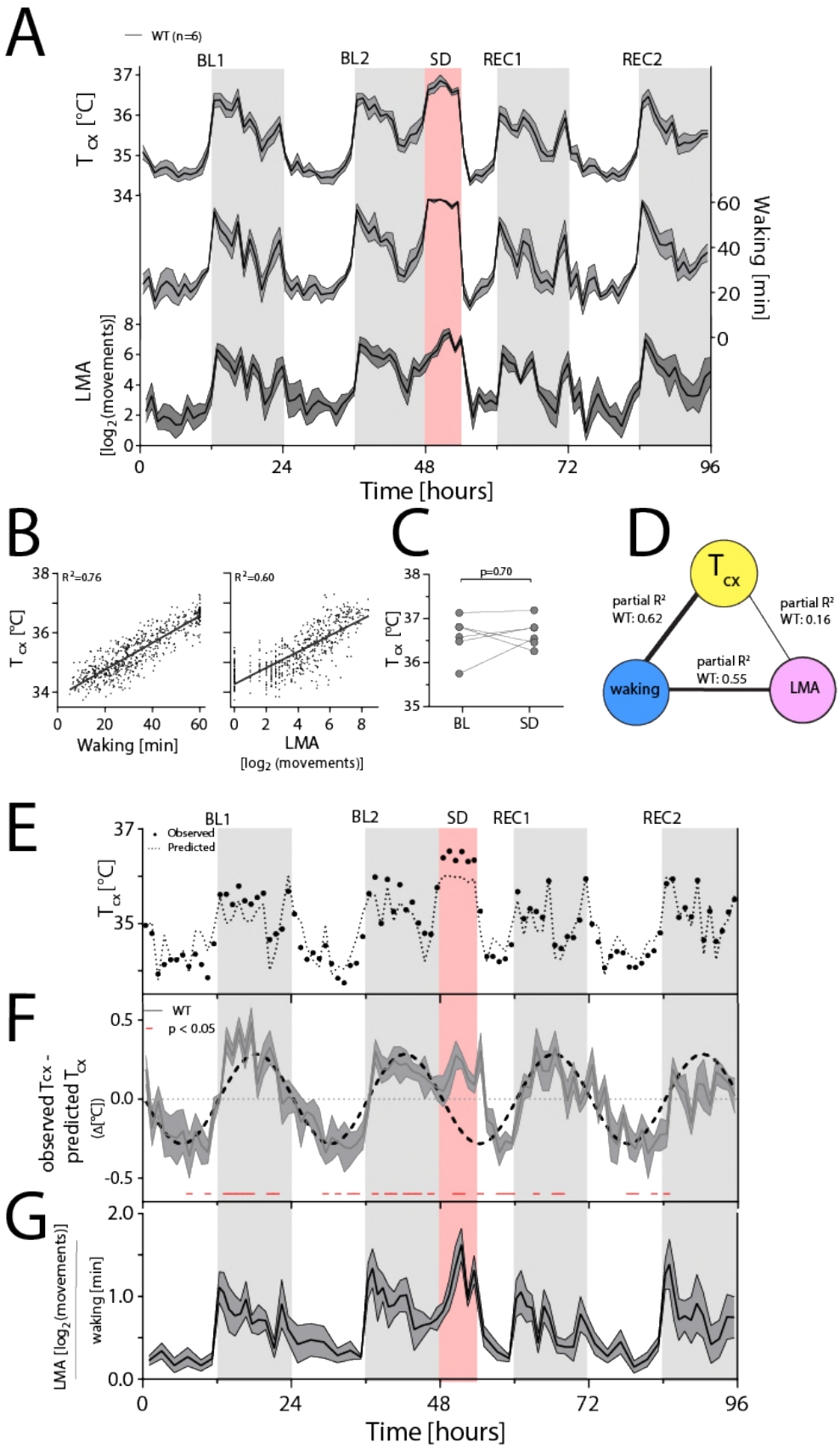

Figure 3: **Waking is the major determinant of T_{cx}.** For panels A, F and G, the dark line represents the mean, areas span ±1SEM. BL: baseline, SD: sleep deprivation, REC: recovery, T_{cx}: cortical temperature, LMA: locomotor activity. **(A)** Time course of hourly values of T_{cx}, waking and LMA across the entire experiment. **(B)** Both waking (left) and LMA (right panel) correlate with T_{cx} (n=6; 96 values per mouse; R^2=0.76 and 0.60, respectively, p<0.0001). **(C)** T_{cx} during SD did not differ from levels reached after long waking bouts during BL (t(5)=0.41, p=0.70). **(D)** Waking after correcting for LMA is the major determinant of T_{cx}, as revealed by partial correlation analysis; here performed on the combined hourly values of all WT mice. **(E)** a representative example [mouse TC03], with measured T_{cx} (closed circles), and predicted T_{cx} (stippled line) [based on the correlation between T_{cx} and waking]. **(F)** During the dark phase and SD, the expected increase in T_{cx} (based on the amount of waking) is lower than the measured T_{cx}, resulting in positive residuals [residuals: observed T_{cx} – predicted T_{cx}], whereas during the light phase, the expected T_{cx} is higher than the measured T_{cx}, resulting in negative residuals (t-test: data<>0, p<0.05). The sinewave was fitted to the residuals during BL1-2. **(G)** LMA per unit of waking follows a similar pattern as the residuals in figure F.

153 Considering the strong correlation between LMA and T_{cx} (WT: R^2=0.72; KO: R^2=0.78; p<0.0001),
154 it could be hypothesized that LMA explains partly the sleep-wake associated changes in T_{cx}. To
155 investigate this further, the respective contribution of waking and LMA to changes in T_{cx} was
156 quantified by a partial correlation analysis. Although LMA did significantly contribute,
157 substantially more of the variance in T_{cx} was explained by waking in both genotypes (paired t-test
158 on Fisher Z-transformed R^2-values from each individual mouse's partial correlation on hourly
159 waking and T_{cx}, and on hourly LMA and T_{cx}: WT: t(5)=5.1, p=0.004; KO: t(5)=10.7, p=0.0001; see also
160 Figure 3-D for R^2-partial correlation coefficients which are based on hourly data from all WT mice
161 combined). We then determined the variance that could not be explained by the correlation
162 between waking to T_{cx} (*i.e.* the residuals) by calculating the difference between the observed T_{cx} in
163 a given hour and the predicted T_{cx} based on the time-spent-awake in that hour. The linear
164 regression overestimated and underestimated T_{cx} during the light phase and dark phase,
165 respectively (Figure 3-E,F; BL1 and BL2), leading to negative residuals during the light phase and
166 positive residuals during the dark phase. Fitting a sinewave through the residuals of the two
167 baseline days revealed a 'circadian' distribution, with a mean amplitude of 0.29°C, which is almost
168 twice the amplitude as was previously reported on in the rat [0.15°C] (Franken et al., 1992).
169 Interestingly, when considering the time course of the residuals throughout the experiment,
170 including the SD and recovery, a consistent parallel with the distribution of LMA expressed per unit
171 of waking became evident (Figure 3-G).
172 Therefore, to determine if including LMA in addition to waking, could predict a larger portion
173 of the variance in T_{cx}, we applied three Mixed Linear Models, where LMA was considered by
174 expressing LMA per unit of waking (LMA/Waking). Model1 explained the variance in T_{cx} based on
175 waking alone, Model2 also incorporated LMA/Waking, and Model3 considered additionally the
176 interaction between Waking and LMA/Waking. Indeed, Model3 predicted best the variance in T_{cx}
177 although in terms of explaining the variance in T_{cx}, the improvement is marginal over the two other
178 models (Model1: R^2_c=0.84; Model2: R^2_c=0.85; Model3: R^2_c=0.86; chi-squared test: Model1 vs Model2:
179 $X^2(5)$=16.2; p<0.0001; Model2 vs Model3: $X^2(6)$=25.0; p<0.0001). Thus, the sleep-wake distribution is
180 the most important determinant of T_{cx} but LMA during waking is modestly contributing as well.
181 Nevertheless, also the residuals of this model, depicted in Figure 3, supplement 1, still showed a
182 similar pattern like the residuals in Figure 3-F, pointing towards the contribution of other
183 (circadian) variables and/or a non-linearity of the association between the contribution of LMA and
184 sleep-wake states to changes in T_{cx}.

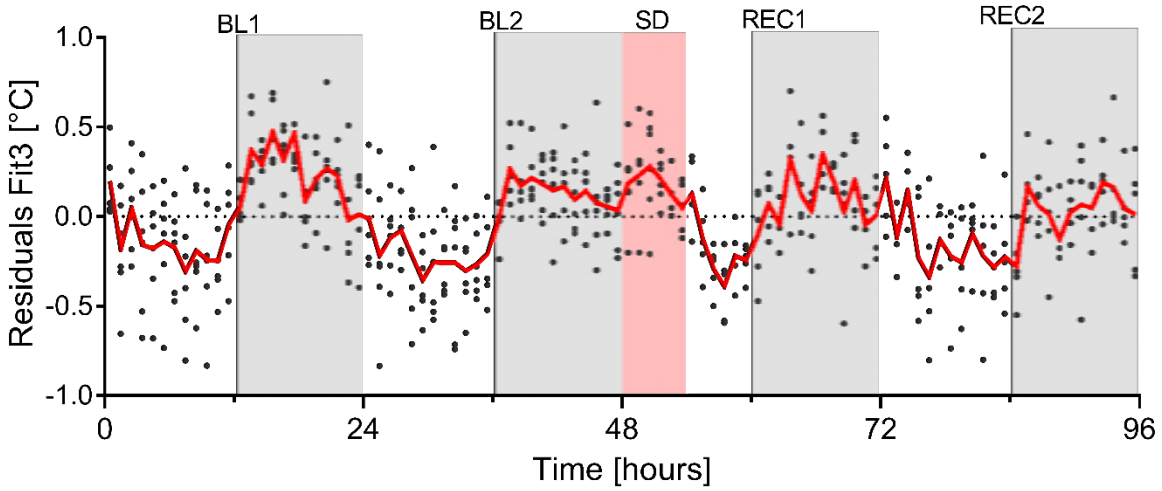

Figure 3, supplement 1 **The residuals of the optimized mixed linear model** (Model3; see Results section) still show a pattern alike the residuals in Figure 3-F. Red line depicts the mean value determined every hour, each dot represents an hourly residual value per mouse.

185

186 THE INFLUENCE OF SD AND CIRBP ON TRANSCRIPTS IN CORTEX AND LIVER

187 After establishing that also in the mouse the sleep-wake distribution is the major determinant
188 of T_{cx}, we assessed whether the SD-incurred changes in CIRBP participate in linking the effect of
189 SD to clock gene expression. To this end, we quantified 11 transcripts from liver and 15 from cortex
190 before and after SD by RT-qPCR. Genes of interest included transcripts affected by SD (Maret et al.,
191 2007, Mongrain et al., 2010) and/or by the presence of CIRBP (Liu et al., 2013, Morf et al., 2012), with
192 an emphasis on clock genes. Mice were sacrificed before SD at ZT0, or 6 hours later after SD (ZT6-
193 SD) together with non-sleep deprived control mice that could sleep *ad lib* (ZT6-NSD). Statistics on
194 ZT0 (t-test) and ZT6 (2-way ANOVA) can be found in Table 1.

195 From ZT0 to ZT6 under undisturbed conditions, T_{cx} decreased because mice spend more time
196 asleep compared to the previous hours in the dark phase (see also Figure 3-A). This decrease in T_{cx}
197 was accompanied by the expected increase of the expression of the cold-induced transcript *Cirbp*
198 in WT mice (cortex: $t(8)=3.2$, $p=0.01$; liver: $t(8)=2.7$, $p=0.03$; Figure 4-A and Figure 4, supplement 1,
199 compare also with the time course of *Cirbp* Figure 1). In contrast, SD during the same time span
200 incurred a decrease in cortical and hepatic *Cirbp* relative to non-sleep deprived controls (cortex:
201 Figure 4-A; liver: Figure 4, supplement 1), consistent with the wake-induced increase in T_{cx} during
202 SD. No *Cirbp* mRNA was detected in KO mice.

203 RBM3 is another cold-inducible RNA Binding Protein and, like CIRBP, conveys temperature
204 cycles into high-amplitude clock gene expression *in vitro* (Liu et al., 2013). A long and a short

205 isoform of *Rbm3* (*Rbm3-long* and *–short*, resp.) that differ in their 3'UTR length were discovered in
206 the mouse cortex. Although both isoforms are referred to as 'cold-induced', they exhibit opposite
207 responses to SD (Wang et al., 2010), with a decrease in the *short* isoform and an increase in the *long*
208 isoform. We found that overall, the short isoform was more common than the long isoform in the
209 cortex (PCR cycle detection number for all samples pooled: cortex: *Rbm3-short*: 25.6±0.2, *Rbm3-*
210 *long*: 29.7±0.1, amplification efficiency *Rbm3-short*: 2.11 and *Rbm3-long* 2.07). In the liver, only the

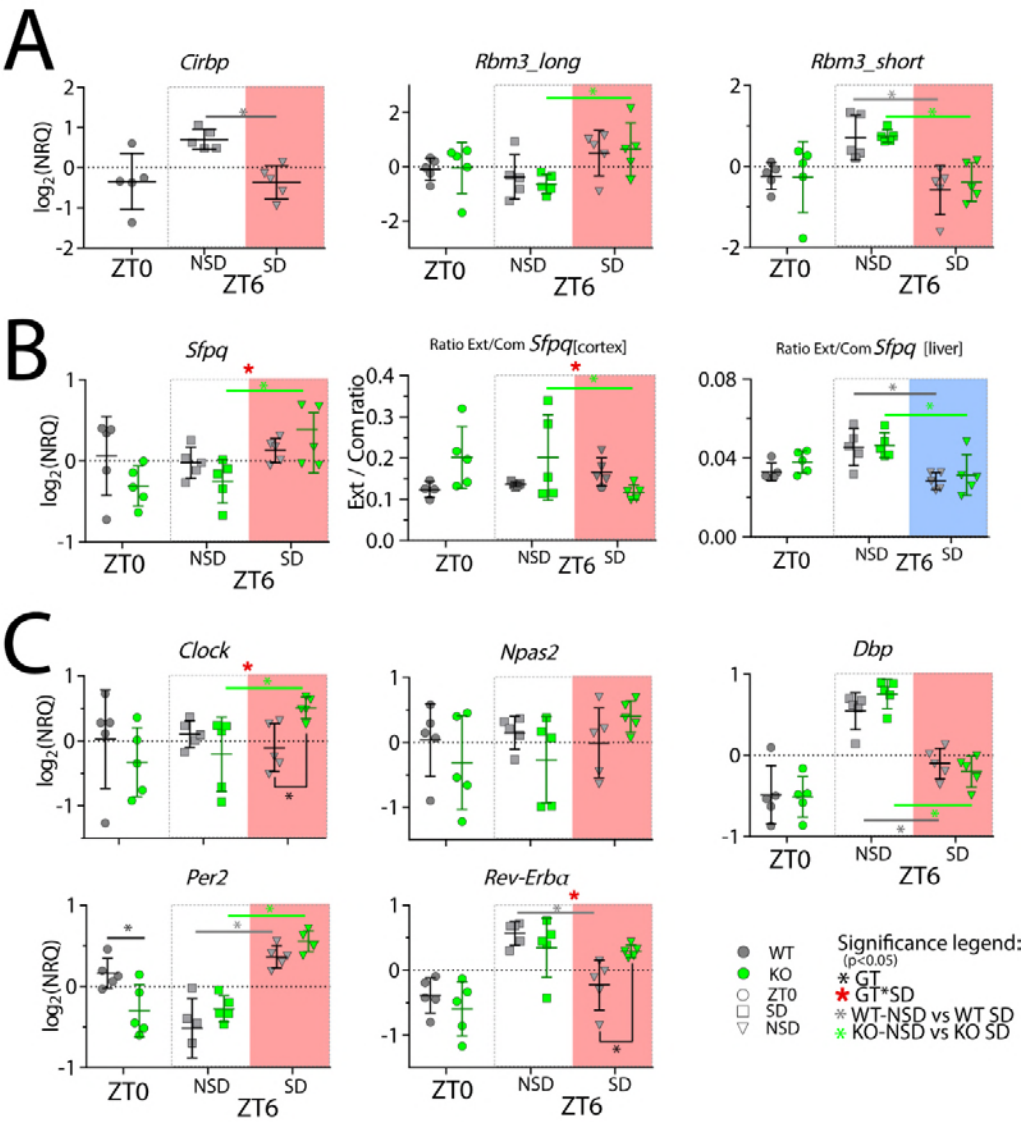

Figure 4 **Cortical expression of several genes is affected by SD and the lack of CIRBP.** NRQ: Normalized Relative Quantity, SD: sleep deprivation, GT: Genotype. n=5 for each group, each symbol represents an observation in one mouse. Mice were sacrificed at ZT0, at ZT6 after sleep deprivation (ZT6-SD) or after sleeping *ad lib* (ZT6-NSD). Statistics are performed separately for ZT0 (factor GT, t-test), and ZT6 (factor GT and SD; 2-W ANOVA). Significant (p<0.05) GT differences are indicated by a black line and *, the effect of SD in WT mice with a grey line and *, and in KO mice with a green line and *. Interaction effects (GTxSD) at ZT6 are indicated by a red *. See Table 1 for statistics.

211 short isoform was detected (liver: *Rbm3-short*: 28.2±0.2, *Rbm3-long*: >32; *i.e.,* beyond reliable
212 detection limit). We confirmed that after SD, *Rbm3-short* was decreased in the cortex (Figure 4-A)
213 and liver (Figure 4, supplement 1), whereas *Rbm3-long* was increased in cortex. The latter
214 observation reached significance only in the KO mice (Figure 4-A).

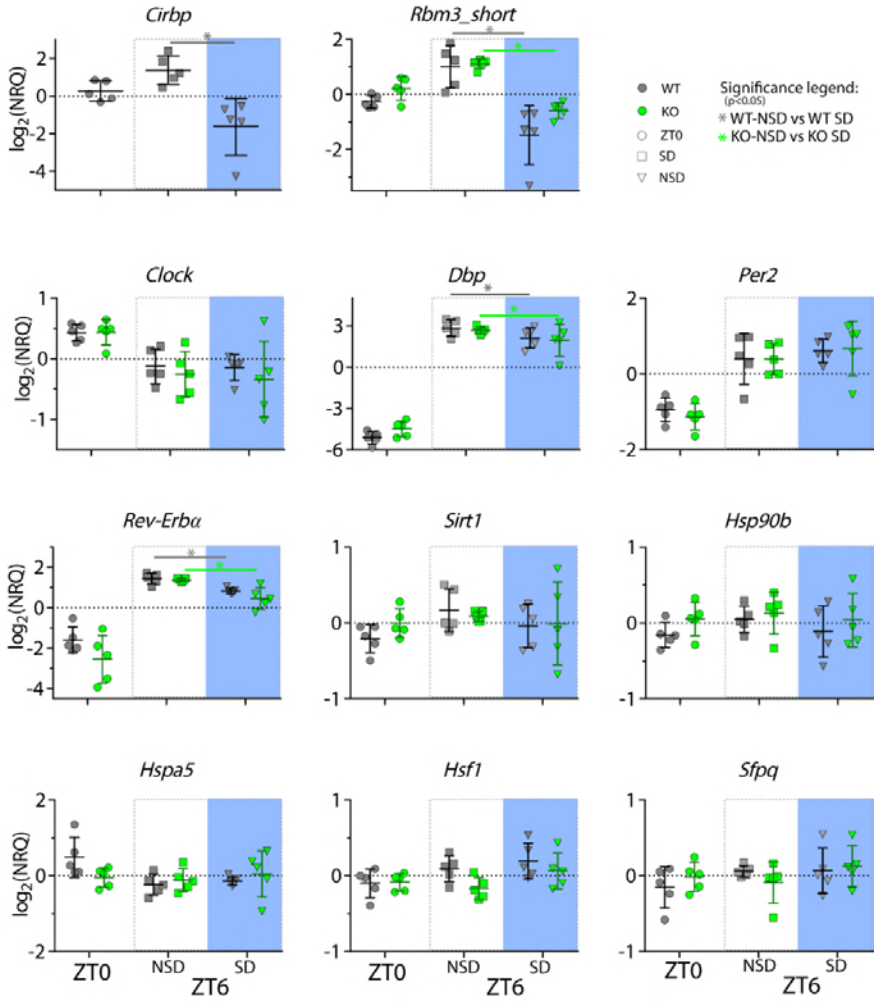

Figure 4, supplement 1 **Changes in transcripts incurred by the absence of CIRBP and/or SD in the liver**. Legend same as in Figure 4. See Table 1 for statistics.

215

216 As anticipated, cortical expression of the activity (and waking)-induced transcripts *Homer1a*,
217 *Dusp4, Hspa5/BiP*, *Hsp90b*, and *Hsf1* was increased by SD (Figure 4, supplement 2). Post-hoc tests
218 revealed that the latter two were significantly increased only in *Cirbp* KO mice. Furthermore, the
219 effect of SD on the transcripts *Hsp90b* and *Hspa5* was significantly amplified in *Cirbp* KO mice
220 compared to WT mice. Unexpectedly, no changes in the expression of heat shock transcripts
221 incurred by SD or genotype were detected in the liver (Figure 4, supplement 1).

222 *In vitro* studies have shown that the presence of CIRBP is associated with longer 3'UTRs of its
223 target genes, such as the transcript splice-factor proline Q (*Sfpq*), resulting in a higher prevalence
224 of long isoforms (extended or *ext*) over all isoforms (common or *com*), and thus an increased
225 *ext/com* ratio [see FigS4-S5 in (Liu et al., 2013)]. We therefore expected a lower *ext/com* ratio in
226 mice lacking CIRBP. However, under baseline conditions [ZT0 and ZT6-NSD], *Cirbp* KO mice did
227 not differ in their *ext/com* ratio from WT littermates (ZT0: liver: ($t(8)=1.55$, $p=0.16$; cortex: $t(7)=2.0$,
228 $p=0.09$; ZT6-NSD: liver: $t(8)=0.19$, $p=0.85$, cortex: $t(8)=1.4$, $p=0.20$). Because also RBM3 partakes in
229 determining the *ext/com* ratio (Liu et al., 2013), the lack of an effect of CIRBP on the *ext/com* ratio
230 could be due to compensation by RBM3. We could test this by assessing the effect of SD on the
231 *ext/com* ratio, because SD acutely suppresses both RBM3 and CIRBP. Indeed, SD significantly
232 decreased the *ext/com* ratio in the liver in both genotypes (Figure 4-B; 2-way ANOVA, factor SD:
233 $F(1,16)=20.4$, $p=0.003$). In the cortex, however, we observed an unexpected non-significant increase
234 in WT mice and a significant decrease in KO mice, leading to a significant GT x SD interaction
235 (cortex: $F(1,16)=5.25$, $p=0.036$). Therefore, our data are inconclusive in confirming a role for CIRBP,
236 and possibly RBM3, in the *in vivo* determination of *Sfpq*'s *ext/com* ratio.

237 Our main question concerned the contribution of CIRBP to sleep-wake induced changes in
238 clock gene expression. Previous studies evaluating the effects of SD on cortical clock transcripts
239 showed a consistent increase in *Per2* and a decrease in *Dbp* and *Rev-erbα*, whereas the response of
240 *Clock* and *Npas2* varied among studies, but if any, tended to increase after SD (reviewed in (Mang
241 and Franken, 2015)). Indeed, in the cortex of WT mice, SD increased cortical *Per2*, decreased *Dbp*
242 and *Rev-erbα* and did not significantly affect *Clock* and *Npas2* (Figure 4-C). In accordance with our
243 hypothesis, CIRBP attenuated the SD induced changes of cortical *Rev-erbα*, a transcriptional
244 repressor recently implicated in the sleep homeostat (Mang et al., 2016). This observation contrasts
245 with the genotype-dependent changes in *Per2*, because when considering the lower levels of cortical
246 *Per2* in *Cirbp* KO mice at ZT0, the effect of SD was amplified (Figure 4-C, 2-way ANOVA, ZT0-
247 ZT6[SD], interaction effect GT x SD: $F(1,16)=12.4$, $p=0.003$). Also, the expression of *Clock* in the
248 cortex was significantly increased by SD in *Cirbp* KO mice and not in WT littermates.

249 Compared to the cortex, the clock gene expression in the liver appeared more resilient to the
250 effects of SD, as only *Dbp* and *Rev-erbα* were significantly affected and not *Per2* (Figure 4,
251 supplement 1). The lack of CIRBP did not interfere with this response, nor did it contribute to
252 genotype dependent changes of other (clock) gene transcripts in the liver.

253 Taken together, the absence of CIRBP modulated the SD induced changes in the cortical
254 expression of the clock genes *Rev-erbα*, *Clock* and *Per2*. Furthermore, the expression of transcripts
255 in the heat shock pathway were also affected in a genotypic manner by SD.
256
257

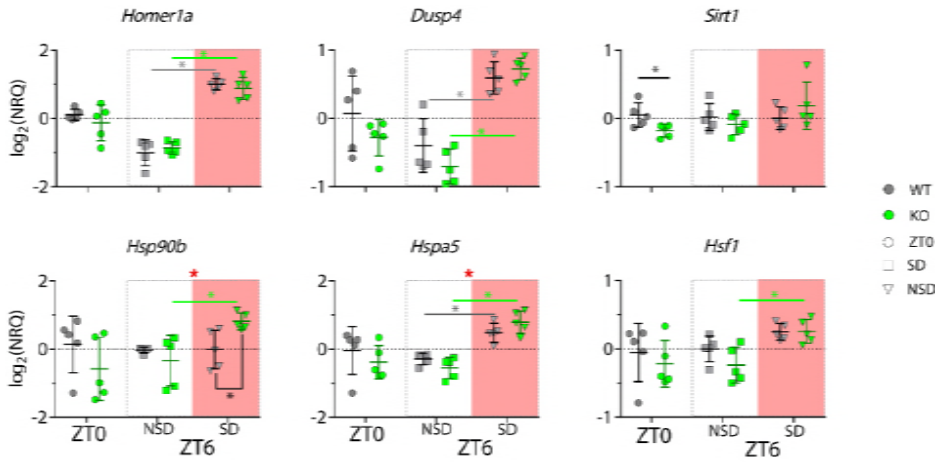

Figure 4, supplement 2 **Changes in transcripts incurred by the absence of CIRBP and/or SD in the cortex**. Legend same as in Figure 4. See Table 1 for statistics.

258 **Table 1**: statistics on RT-qPCR results

	Cortex				Liver			
		ZT6				ZT6		
Transcript	ZT0 (#)	SD/NSD(*)	GT (*)	Interaction (*)	ZT0 (#)	SD/NSD (*)	GT (*)	Interaction (*)
Cirbp	X	**t(8)=4.9; p=0.001**	X	X	X	**t(8)=4.0, p=0.004**	X	X
Clock	t=0.86; p=0.21	F=2.38; p=0.14	F =0.85; p=0.37	**F=8.02; p=0.01**	t=0.03; p=0.98	F=0.09; p=0.77	F=0.81; p=0.38	F=0.03; p=0.87
Dbp	t= 0.13; p=0.90	**F=82.0; p<0.0001**	F=0.39; p=0.54	F=3.06; P=0.10	t=1.99; p=0.08	**F= 4.37; p=0.05**	F=0.23; p=0.64	F=0.0002; p=0.99
Dusp4	t=1.29; p=0.23	**F=97.55; p<0.0001**	F=0.50; p=0.49	F=3.24; P=0.09	X	X	X	X
Homer1a	t=0.96; p=0.36	**F=228.8; p<0.0001**	F=0.005; p=0.94	F=1.08; P=0.31	X	X	X	X
Hsf1	t=0.67; p=0.52	**F=18.22; p=0.0006**	F=1.79; p=0.20	F=1.9; P=0.18	t=0.14; p=0.89	F=3.43; p=0.08	F=4.63; p=0.05	F=0.48; p=0.50
Hsp90b	t=1.29; p=0.23	**F=7.18; p=0.0164**	F=1.40; p=0.25	**F=6.86; p=0.02**	t=1.71; p=0.12	F=0.93; p=0.35	F=0.80; p=0.38	F=0.07; p=0.80
Hspa5	t=0.89; p=0.40	**F=72.03; p<0.0001**	F=0.03; p=0.86	**F=5.32; p=0.03**	t=2.02; p=0.08	F=0.62; p=0.44	F=0.84; p=0.37	F=0.04; p=0.86
Npas2	t=0.86; p=0.41	F=1.56; p=0.2298	F=0.0008; p=0.98	F=3.99; p=0.06	X	X	X	X
Per2	**t=2.78; p=0.02**	**F=75.22; p<0.0001**	**F=4.78; p=0.04**	F=0.06; p=0.80	t=0.90; p=0.40	F=0.95; p=0.34	F=0.01; p=0.92	F=0.02; p=0.90
Rbm3-short	t=0.05 ; p=0.96	**F=32.04 ; p<0.001**	F=0.31; p=0.59	F=0.13; p=0.73	t=2.23; p=0.06	**F=47.6; p<0.0001**	F=2.7; p=0.12	F=1.6; p=0.22
Rbm3-long	t=0.10 ; p=0.92	**F=9.49 ; p=0.007**	F=0.03; p=0.86	F=0.32; p=0.58	X	X	X	X
Rev-erbα	t=0.91; p=0.39	**F=8.95; p=0.009**	F=1.09; p=0.31	**F=6.80; P=0.02**	t=1.59; p=0.15	**F=31.13; p<0.0001**	F=2.41; p=0.14	F=1.37; p=0.26
Sfpq	t=1.51; p=0.17	**F=11.61; p=0.004**	F=0.017; p=0.90	**F=4.44; p=0.05**	t=0.93; p=0.38	F=1.26; p=0.28	F=2.78; p=0.11	F<0.001; p=0.98
Sirt1	**t=2.56; p=0.04**	F=1.61; p=0.22	F=0.14; p=0.72	F=2.07; p=0.17	t=1.75; p=0.12	F=0.94; p=0.35	F=0.03; p=0.87	F=0.12; p=0.73

259

260

261 GT: genotype, SD/NSD: Sleep deprived / non-sleep deprived (control)

262 ZT0: t-test, degrees of freedom: 8

263 ZT6: two-way ANOVA (factors SD and GT), df=1 for both factors SD, GT and its interaction; error df=16

264 X: Ct>30 or undetected

265 Green: significant decrease (at ZT0: KO relative to WT; at ZT6, SD/NSD: SD relative to NSD; GT: KO relative to WT)

266 Red: significant increase (at ZT0: KO relative to WT; at ZT6, SD/NSD: SD relative to NSD; GT: KO relative to WT)

267 Purple: significant interaction

268 Significance level: α=0.05

269

270

271

272

CIRBP CONTRIBUTES TO SLEEP HOMEOSTASIS

Because *Cirbp* KO mice showed a modulated response to SD in three out of the five cortical clock gene transcripts we quantified, and clock genes importantly partake in the sleep homeostatic process (reviewed in (Franken, 2013)), we hypothesized that *Cirbp* KO mice have a blunted sleep-homeostatic process. We quantified EEG power in the delta band [0.75 – 4.0 Hz] during NREM sleep, which is a proxy of NREM sleep pressure and reflects a homeostatically regulated sleep process, Process S (Daan et al., 1984). As additional sleep homeostatic measures, we calculated the amount of NREM and REM sleep recovered after SD relative to baseline sleep.

Baseline characteristics of sleep-wake behavior do not differ between Cirbp KO and WT mice

During the two baseline days, no significant differences in waking, NREM or REM sleep were observed. This was neither the case for time spent in these three behavioral states per light and dark phase (Table 2), nor for the distribution of sleep and waking across the day (see Figure 5-A and Figure 6-A). Noteworthy is that under constant darkness we did not detect a change in circadian period length (period (hours): WT (n=5): 23.8±0.03 and KO (n=7): 23.8±0.01).

	WT		KO		Statistics (2-way ANOVA)
	Light	Dark	Light	Dark	Factor GT x Light, Df : 1,35
NREM sleep	389±4	189±10	376±4	170±13	F=0.02, p=0.89
REM sleep	70±2	19±2	66±2	20±2	F=0.83, p=0.37
Total waking	260±4	512±11	277±5	530±14	F=0.02, p=0.90
TDW	45±3	179±12	55±5	192±15	F=0.13, p=0.72
LMA	119±16	817±70	181±26	1370±142	F=7.1, p=0.01

Table 2. Baseline time spent in sleep-wake states (min) and LMA (movements) per 12 hours per genotype, averages of BL1-2. 2-way ANOVA (Factor GT and Light/Dark) on those same 12-hour values. Degrees of freedom for both GT and Light/Dark: Df=1; error term: Df=35.

Sleep homeostatic processes under baseline and recovery

The time course of delta power in the two genotypes was overall similar. In the dark phase, when mice spent most of their time awake and thus sleep pressure accumulates, delta power during NREM sleep was highest. This contrasts with the end of the light phase [ZT8-12], where NREM sleep delta power reached its lowest levels of the day due to the high and sustained prevalence of NREM sleep in the preceding hours. Despite the overall similarities in daily changes of NREM delta power, subtle differences were observed: delta power levels were higher during the dark phase in *Cirbp* KO compared to WT mice, and these differences reached significance during the dark periods of recovery (Figure 5-A, 2nd graph from top).

298 Differences in delta power can be attributed to changes in the dynamics of the underlying
299 homeostatic process, Process S, and/or to changes in the sleep-wake distribution. Evidence
300 supporting the latter possibility was observed because *Cirbp* KO mice tended to spend less time in
301 NREM sleep (and more time awake) during the early dark phase compared to WT mice, reaching
302 significance during the recovery (Figure 5-A; 3rd graph from top). To test if these changes in the
303 sleep-wake distribution were indeed sufficient to raise NREM delta power above WT levels, we
304 estimated the increase (τ_i) and decrease (τ_d) rate of delta power by a simulation of Process S based
305 on the sleep-wake distribution. We assumed Process S to increase exponentially during waking and
306 REM sleep by time constant τ_i and to decrease during NREM sleep by time constant τ_d (see Materials

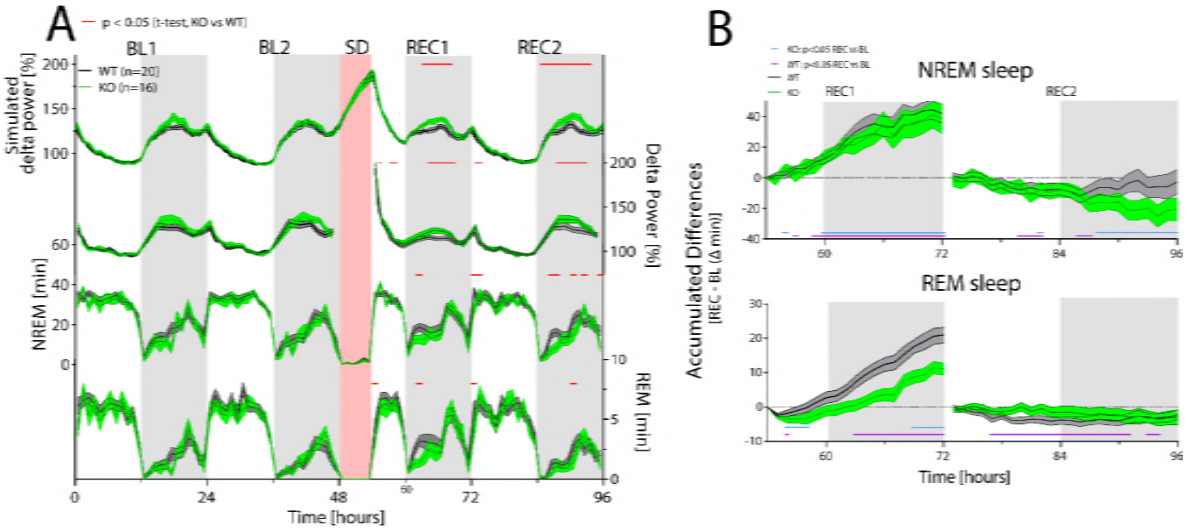

Figure 5 **CIRBP modulates the sleep-wake distribution and REM sleep recovery after sleep deprivation.** *Cirbp* KO (green lines and areas) and WT (black line, grey areas) mice during the two baseline days (BL1 and -2), sleep deprivation (SD), and the two recovery days (REC1 and -2; areas span ±1SEM range). **(A)** From top to bottom: Simulated delta power (Process S), measured NREM delta power, NREM sleep and REM sleep. During BL, trends, but no significant effect of GT or its interaction with time were detected in the simulation of process S, delta power, NREM sleep or REM sleep. During REC, the simulation predicts increased delta power in *Cirbp* KO mice (GT: F(1,34)=5.56, p=0.024), based on differences in NREM sleep distribution (GT: F(1,34)=6.02, p=0.0194) which are also reflected by increased delta power during the dark phase (GT: F(1,34)=4.65, p=0.038). GT effects in REM sleep were also detected during recovery (factor GT: F(1,34)=5.45, p=0.026). Exact timing of GT differences is indicated by superimposed red lines (post-hoc t-test, p<0.05). **(B)** Top: KO mice recover as much NREM sleep as WT mice in the first 18hrs after SD (REC1 at 72Hr: WT: 41.9±6.1 KO: 38.6±9.7 min; t-test: t(34)=0.30, p=0.76). Bottom: KO mice accumulated less REM sleep during the first recovery day over the baseline day in comparison to WT mice relative to baseline (REC1 at 72Hr, WT: 20.9±2.3 KO: 9.9±2.0, t-test: t(34)=3.7, p=0.0007).

307

308 and Methods, and (Franken et al., 2001) for more details). This simulation not only captured
309 well the overall dynamics (mean square of the measured-predicted differences, mean±SEM: WT:
310 10.1±0.3, KO: 10.4±0.4) but also the genotype differences in delta power (Figure 5-A; top graph). No
311 differences in the time constants of Process S were detected (see Table 3). Hence, the reduction in
312 NREM sleep in *Cirbp* KO mice in the beginning of the dark period caused the higher NREM EEG

313 delta power values in subsequent hours, underscoring the notion that small differences in NREM
314 sleep time can have large repercussions on delta power when waking prevails and thus Process S
315 increases (Franken et al., 2001).

	WT	KO	t-test, df=34
S_o [%]	128.2 ± 2.4	132.1 ± 2.6	t=1.10, p=0.29
τ_i [h]	13.2 ± 1.2	12.9 ± 1.0	t=-0.16, p=0.87
τ_d [h]	3.0 ± 0.2	2.8 ± 0.2	t=-0.74, p=0.46
LA [%]	45.1 ± 1.4	45.1 ± 1.1	t=-0.02, p=0.98
UA [%]	288.8 ± 3.0	296.6 ± 3.2	t=1.80, p=0.09

Table 3 **Time constants, asymptotes and S_o for Process S do not differ between *Cirbp* WT and KO mice.** Mean time constants (±SEM) obtained by the simulation (Process S) with the best fit to the NREM delta power values, where the increase of Process S is simulated by τ_i, the decrease by τ_d and the upper- and lower asymptotes by UA and LA, respectively. No significant genotype differences were observed. See material and methods for detailed description of the simulation.

316 A different aspect of NREM sleep homeostasis concerns the regulation of time spent in this state.
317 This can be quantified by accumulating relative differences in time spent in NREM sleep from
318 corresponding baseline hours over the recovery period. At the end of the first recovery day, both
319 KO and WT mice had gained ca. 40 minutes of NREM sleep relative to baseline (Figure 5-B, upper
320 panel).

321 The amount of REM sleep is also homeostatically defended (Franken, 2002). At the end of REC1,
322 both WT and KO mice spent more time in REM sleep compared to corresponding baseline hours.
323 However, this increase in REM sleep was significantly attenuated by 46% in *Cirbp* KO mice (Figure
324 5-B, lower panel). Because no significant differences were detected during baseline in time spent in
325 REM sleep (see also Table 1), this attenuated rebound in REM sleep resulted from less REM sleep
326 during recovery, specifically in the first hours of the dark phase when the genotypic differences
327 were most prominent (Figure 5-A, lowest graph).

328 Thus, although CIRBP did not affect the processes underlying NREM sleep intensity and NREM
329 sleep time, it did contribute to REM sleep homeostasis by increasing the amount of REM sleep after
330 SD.

331

332 AN UNANTICIPATED WAKING PHENOTYPE IN CIRBP KO MICE

333 While quantifying sleep-wake states, we observed that *Cirbp* KO mice were more active than
334 their WT littermates during the dark phase (t(31)=-2.56, p=0.015, see also Table 2). More specifically,
335 *Cirbp* KO mice were almost twice as active in the first 6hrs of the dark phase (movements: WT:

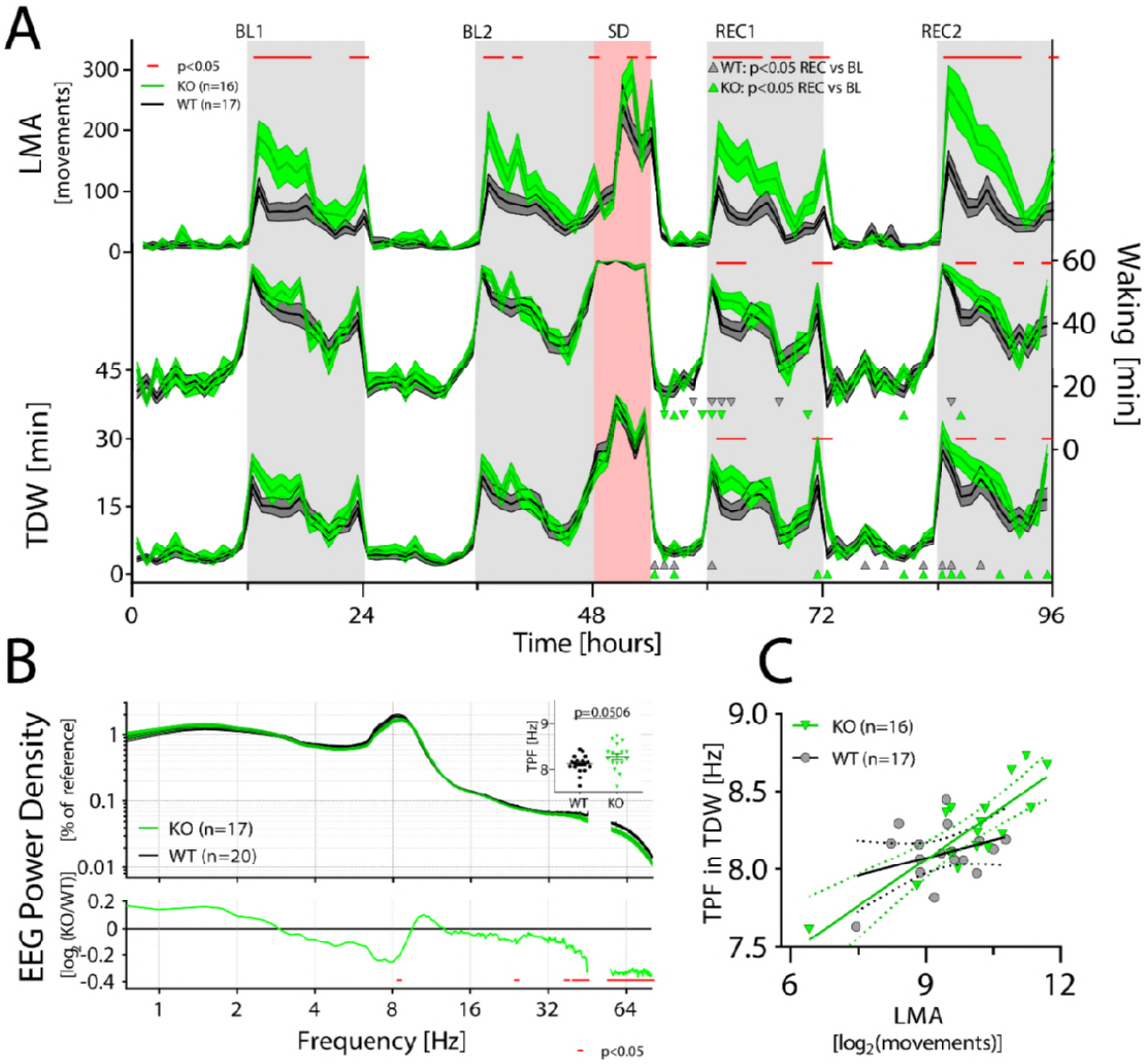

Figure 6 **CIRBP suppresses LMA and affects spectral composition during TDW**. LMA: locomotor activity, TDW: theta dominated waking; TPF: theta peak frequency. (A) *Cirbp* KO (green lines and areas) and WT (black line, grey areas) mice during the two baseline days (BL1 and -2), sleep deprivation (SD), and the two recovery days (REC1 and -2; areas span ±1SEM range). **(A)** *Cirbp* KO mice are more active in the dark periods only (BL: GTxTime: F (47, 1457) = 3.5, P<0.0001; REC: GTxTime: F (41, 1271) = 5.2, P<0.001), and spent more time awake and in theta dominated waking (TDW) during REC compared to WT mice (total waking: BL: GTxTime: F(47,1457)=1.1, P=0.33 REC: GTxTime: F (41, 1271) = 1.9, P=0.0005; TDW: BL: GTxTime: F (47, 1457) = 1.1, P=0.35; REC: GTxTime: F (41, 1271) = 1.8, P=0.0025). Significant genotype differences are marked superimposed red lines (post-hoc t-tests; p<0.05). Δ and ∇ indicate a significant increase and decrease in REC compared to same time in BL, respectively. **(B)** CIRBP contributes to the spectral composition of TDW in the dark phase (2-way RM ANOVA; GTxFreq: F(278,9730)=2.0; p<0.0001, red symbols in lower panel: post-hoc t-tests, p<0.05), and KO mice tend to have faster TPF during TDW in the dark phase (t(35)=2.0; p=0.0506). **(C)** TPF in the dark phase correlates only in the KO mice significantly with LMA (WT: R^2=0.12, p=0.17, KO: R^2=0.71, p<0.0001).

336

337 463.8±60.7, KO: 801.8±118.4, t(35)=-2.7, p=0.012; Figure 6-A). Interestingly, this pronounced
338 increase was not associated with a significant increase in time spent awake during BL (per 12 hrs:
339 t(35)=1.2, p=0.24, and see Table 2), and indeed *Cirbp* KO mice were more active per unit of waking
340 (average in the dark phase, LMA [movements/waking(min)], WT: 1.3±0.13, KO: 2.1±0.28; t(35)=-2.7,

341 p=0.01). Note that also T_{cx} was not significantly increased in *Cirbp* KO mice during the dark phase
342 (T_{cx}: WT: 35.9±0.1, KO: 36.1±0.1, t-test, t(10)=1.3, p=0.24) despite the increased LMA at this time of
343 the day, again underscoring the minimal contribution of LMA to T_{cx}.

344 Because *Cirbp* KO mice are not more awake (Table 2 and Figure 6), we wondered if their
345 increased LMA is associated to the prevalence of sub-states of waking. Theta-dominated waking
346 (TDW) is a sub-state of waking that correlates with activity, prevails during the dark phase and SD,
347 and is characterized by the presence of EEG theta-activity (Buzsáki, 2006, Vassalli and Franken,
348 2017). Despite their increased LMA, *Cirbp* KO mice did not spend more time in TDW during the
349 dark phase of the BL (see Table 1, t(31)=-1.22, p=0.23). If not time spent in TDW, does the increased
350 LMA in *Cirbp* KO mice relate to changes in brain activity during dark phase TDW?

351 Although in both genotypes the TDW EEG showed the characteristic theta activity [6.5-12.0
352 Hz], subtle differences between genotypes were detected in the spectral composition of the EEG
353 signal. Slow [32-45Hz] and fast [55-80Hz] gamma power were both reduced during TDW in *Cirbp*
354 KO mice (Figure 6-B), and this reduction was observed throughout the experiment (Figure 6,

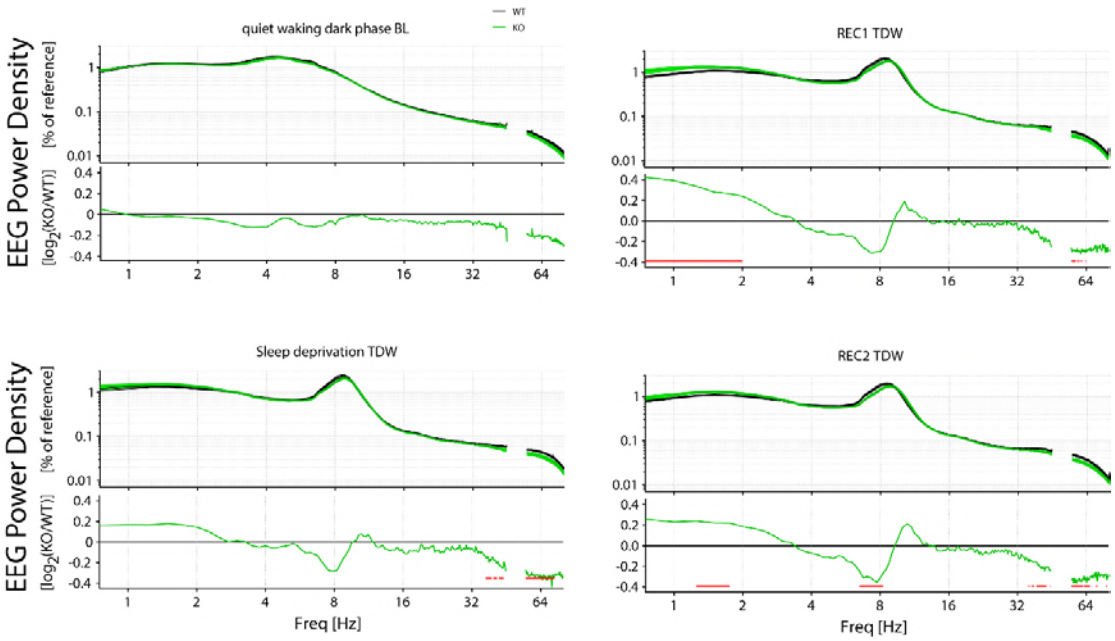

Figure 6, supplement 1 **Changes in the EEG spectra are observed in TDW, but not in quiet waking.** Spectral composition of *Cirbp* KO (green lines and areas; n=17) and WT (black line, grey areas; n=20) mice at different times of the experiment (indicated by the title, BL: baseline, REC1: recovery1, REC2: recovery2). In each graph, the top panel depicts the spectral composition whereas in the lower panel, the KO spectral composition relative to the WT is shown (ratio KO/WT). Red symbols in lower panel indicate significant difference for the frequency bins (post-hoc t-test, p<0.05). 'Quiet' waking baseline dark phase: No effect of GT or an interaction effect (2-way RM ANOVA, GT*Freq: F(278, 9730)=0.81, P=0.99) on the spectral composition of quit waking in the dark phase of the baseline. Sleep deprivation TDW: significant interaction between GT and Freq (F (278, 9730) = 1.722, P<0.0001). REC1 TDW: significant interaction: F (278, 9730) = 2.984, P<0.0001; REC2 TDW: significant interaction F(278, 9730)=3.083, P<0.0001).

355 supplement 1; and see time course in Figure 6, supplement 2), indicating that these spectral
356 genotype differences are robust across different light conditions, circadian times and throughout
357 the SD.
358 In contrast, the spectral composition of the EEG during 'quiet' waking (*i.e.* all waking that is not
359 TDW) was remarkable similar between the two genotypes (Figure 6, figure supplement 1),
360 demonstrating that the changes in spectral composition of TDW EEG are not the result of a general
361 effect of CIRBP on the waking EEG.
362 Moreover, we observed a decrease in slow and a non-significant increase in faster theta
363 activity in the TDW EEG of *Cirbp* KO mice, together hinting at an acceleration of theta peak
364 frequency (TPF; lower panel in Figure 6-B). TPF during TDW in BL was indeed increased in KO
365 mice (+0.15Hz) although our significance threshold was not met ($t(35)=2.0$, $p=0.0506$). No
366 suggestions for accelerated TPF in REM sleep during BL, the other sleep-wake state characterized
367 by distinct theta oscillations in the EEG, were detected (WT: 7.43±0.06; KO: 7.56±0.05, $t(35)=1.7$,
368 $p=0.10$). During locomotion, increased LMA correlates well with increased TPF (Jeewajee et al.,
369 2008). In accordance with this observation, mean $\log_2$-transformed LMA levels per mouse during
370 the dark phase predicted well the mean TPF observed during TDW at the same time of day (WT
371 and KO combined; $R^2=0.52$, $p<0.0001$), although this relationship remained significant only in KO
372 mice when assessing the two genotypes separately (Figure 6-C). This genotype-dependent
373 association between TPF and LMA was not confirmed by a significant difference in slope between
374 the genotypes (ANCOVA, $F(1,29)=3.8$, $p=0.059$).
375 Because the group correlation did not account for inter-individual differences in LMA levels, we
376 also assessed the correlations between TPF and LMA within individual mice. Moreover, to test if
377 this association depended on the lighting condition, we analyzed this during the dark and light
378 phase separately (*i.e.* 24 values per mouse per lighting condition; see also Table 4). In the dark
379 phases, this correlation was significant in all but one mouse (a KO), and both the slope and the
380 predictive power of this correlation did not significantly differ between genotypes (slope: WT:
381 0.15±0.01, KO: 0.14±0.01, $t(31)=0.37$, $p=0.72$; R^2: WT: 0.81±0.03; KO: 0.79±0.04, t-test on the Fisher Z-
382 transformed R^2-values: $t(31)=-0.49$, $p=0.62$). In the light phases, this association was weaker

383
384

TPF during BL	WT	KO
Light	7.77±0.03	7.64±0.04
Dark	8.13±0.04	8.28±0.07

Table 4: Average TPF during baseline light and dark (mean ± SEM) in TDW

385

386 (dark vs. light: paired t-test: slope: t(32)=7.8, p<0.0001; Fisher Z-transformed R^2-values: t(32)=5.9,
387 p<0.0001), but again did not differ between genotypes (WT: 0.07±0.01, KO: 0.09±0.01, t(31)=1.2,
388 p=0.23; R^2: WT: 0.59±0.04; KO: 0.67±0.05, t-test on the Fisher Z-transformed R^2-values: t(31)=1.2,
389 p=0.23). However, during the light phases, when LMA and TDW are substantially reduced and
390 estimates of TPF during TDW are less precise, we found more non-significant associations in both
391 genotypes (KO: 3/ 16; WT: 3/ 17 mice). Altogether, these results provide further evidence that LMA
392 contributes to TPF and suggests that CIRBP, through its effects on LMA, reduces TPF.

393 The SD altered the distribution of waking during the recovery relative to BL (3-way RM ANOVA,
394 factor Time, GT and BL/REC, factor BL/REC: REC1: F(1,558)=42.7, p<0.0001; REC2: F(1,1514)=441.8,
395 p<0.0001; see triangles in REC1 and REC2, Figure 6-A). Surprisingly, while time spent awake was
396 overall decreased compared to baseline, we observed several intervals during the recovery in which
397 TDW was increased (3-way RM ANOVA, factor Time, GT and BL/REC, factor BL/REC: REC1:
398 F(1,558)=13.9, p=0.0002; REC2: F(1,1514)=233.8, p<0.0001; Figure 6-A, upwards pointing triangles).
399 This was true for both genotypes. Moreover, genotype differences in the distribution of waking and
400 TDW became significant during the dark phases of both recovery days, with *Cirbp* KO mice
401 spending more time awake and in TDW than WT mice (Figure 6-A; see post-hoc tests indicated by
402 red line), as if SD amplified the non-significant genotype differences during BL (3-way RM ANOVA
403 on hourly values: factor GTxTimexSD: total waking: F(41,1271)=1.4, p=0.04; TDW: F(41,1271)=1.4,
404 p=0.056) but not for LMA (F(41,1271)=1.0, p=0.48).

405 The EEG spectra during TDW in REC1 and REC2 showed similar profiles as during BL (see Figure
406 6, figure supplement 2), although there were some changes that in recovery reached significance

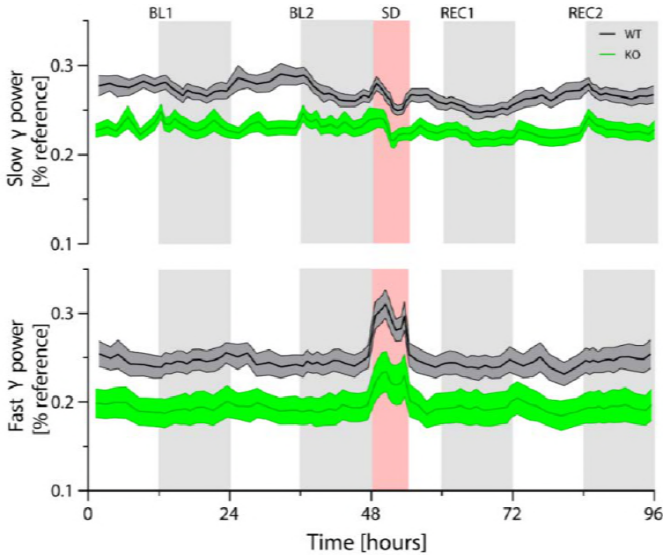

Figure 6, supplement 2 **Slow and fast gamma power over the course of the experiment.** *Cirbp* KO (green lines and areas) and WT (black line, grey areas) mice (areas span ±1SEM range). BL: baseline, SD: Sleep deprivation, REC: Recovery. Power in both slow [32-45Hz] and fast [55-80Hz] gamma is significantly reduced over the course of the experiment in *Cirbp* KO mice (2-way ANOVA: factor GT: slow gamma: F(1,34)=11.9, p=0.002; fast gamma: F(1,33)=6.6, p=0.01). Like the analysis of delta power, power in the gamma bands is calculated based on intervals to ensure an equal contribution of epochs to each time point: 6 intervals in the light phase, 12 in the dark periods, 8 in the sleep deprivation and 4 during the recovery light period.

such as the increase in the delta power band. Along those lines, the non-significant increase in TPF in *Cirbp* KO mice during the BL dark phases became significant in the REC dark phases (REC1: WT: 8.1±0.05, KO: 8.4±0.07, $t(35)=2.7$, $p=0.01$; REC2: WT: 8.2±0.05, KO: 8.5±0.08, $t(35)=2.6$, $p=0.01$). Also, the non-significant difference in slope at the group level between TPF and LMA during BL (Figure 6-C), became significant after SD (ANCOVA, $F(1,29)=5.8$, $p=0.02$), providing further evidence that the suggestive genotype differences under baseline conditions become more pronounced after a challenge of the sleep homeostat.

Taken together, *Cirbp* KO mice were more active during the dark phase, which partly explains the faster TPF. Moreover, KO mice had less EEG power in the gamma band of TDW, and the 6-hour SD strengthened genotype differences in the sleep-wake distribution and EEG activity.

Discussion

In this study, we showed that, like in other rodents, the sleep-wake distribution is the major determinant of T_{cx} in the mouse. Because of the well-established link between temperature and CIRBP levels, it is likely that the equally well-known sleep-wake driven changes in *Cirbp* expression in the brain are conveyed through the sleep-wake driven changes in brain temperature. As predicted, the SD-incurred changes in the expression of clock genes was modulated by the presence of CIRBP. However, only for *Rev-Erbα* did we observe the anticipated attenuated response to SD in *Cirbp* KO mice, whereas the changes in the expression of *Per2* and *Clock* were amplified compared to WT mice. Moreover, we did discover evidence of altered dynamics of the process regulating time spent in REM sleep. Unexpectedly, *Cirbp* KO mice are more active during the dark phase, and have during TDW reduced power in the gamma band and increased TPF.

CHANGES IN CORTICAL TEMPERATURE ARE SLEEP-WAKE DRIVEN

When sleep and waking occur at their appropriate circadian times, the changes in both brain and body temperature have a clear 24-hour rhythm and therefore appear as being controlled directly by the circadian clock. However, sleep-wake cycles contribute significantly to both the daily changes in brain and body temperature. In humans, this involvement is powerfully illustrated by spontaneous desynchrony, where body temperature follows both a circadian and an activity-rest (and presumably, sleep-wake) dependent rhythm (Wever, 1979). The contribution of sleep-wake state to the daily dynamics in body temperature is further supported by forced desynchrony studies, such as (Dijk and Czeisler, 1995), estimating that 'masking' effects of rest-activity and sleep-wake cycles contributed between 30% and 50% to the amplitude of the circadian body temperature rhythm (Hiddinga et al., 1997, Dijk et al., 2000). Not only in humans but also in smaller animals like rats, a circadian and rest-activity component contribute to the circadian fluctuations in body temperature (Cambras et al., 2007). Thus, the circadian amplitude of body temperature is amplified when wake and sleep occur at the appropriate phase of the circadian rhythm.

In contrast to body temperature, brain temperature in rodents is much more determined by sleep-wake state: 80% of its variance can be explained by the sleep-wake distribution ((Franken et al., 1992) and this study). Likewise, the sleep-wake driven changes in brain temperature are still present in arrhythmic animals (Edgar et al., 1993, Baker et al., 2005), pointing to a more important sleep-wake dependency of brain temperature compared to body temperature. In our study, we also

449 estimated the contribution of LMA to changes in T_{cx} and found that waking with higher LMA is
450 associated with higher T_{cx}. Although significant, the contribution of LMA to the daily changes in
451 T_{cx} was modest and explained only 2% more of the variance compared to waking alone. Can we
452 optimize the prediction of T_{cx}? A non-linear relationship between sleep-wake state and T_{cx} was
453 assumed previously (Franken et al., 1992) and could have improved the prediction of our model
454 further. This is supported by the residuals from the complete model (see Figure 3, supplement 2),
455 that exhibit under baseline conditions a circadian distribution, whereas during the SD, they remain
456 increased as during the dark phase. Thus, the model overestimates T_{cx} during periods with little
457 waking (light phase) and underestimates T_{cx} during periods that are dominated by waking (dark
458 phase and SD), suggesting a non-linear relationship between these two variables.

459 Important to consider is that the influence of LMA on T_{cx} is likely affected by the type of activity;
460 for example, rats on a running wheel activity can increase their brain temperature by 2°C within 30
461 minutes (Fuller et al., 1998). Also exercise in men leads to an increase in (proxies) of brain
462 temperature (Nybo et al., 2002). Thus, although in our study the effect of LMA to T_{cx} was very
463 modest compared to the effect of waking on T_{cx}, these contributions likely differ with various types
464 of physical activity.

465

466 LMA-DEPENDENT AND INDEPENDENT CHANGES IN WAKING CHARACTERISTICS

467 Little is known about the role of CIRBP in neuronal and behavioral functioning. It was therefore
468 unanticipated that *Cirbp* KO mice were more active during the dark phase. Neither were the
469 changes in neuronal oscillations during TDW: a reduction in low- and high gamma power and an
470 increase in TPF. Because increased running speed correlates with increased hippocampal TPF
471 (Jeewajee et al., 2008), and our measured TPF is mainly of hippocampal origin (Buzsáki, 2006), we
472 indeed can relate the increased TPF to the increase in LMA in KO mice. In contrast to TPF, the
473 literature has not consistently reported on a relation between the general decrease in gamma power
474 during active waking and its relation to LMA. Some studies have found that increased speed of
475 movement relates to increased power in the gamma band (Furth et al., 2017, Niell and Stryker, 2010,
476 Vinck et al., 2015), whereas others found that this association is only present in higher gamma
477 frequencies [>60Hz] (Zheng et al., 2015). Thus, it is unclear if LMA relates to changes in gamma
478 power. However, there is a clear increase in power of the high gamma band specifically during the
479 SD (see Figure 6, supplement 2), as noted previously (Vassalli and Franken, 2017). This increase was
480 present in both genotypes suggesting that while KO mice seem to have a reduced capacity to

481 produce fast gamma activity, SD is still able to activate their fast-gamma circuitry. These results,
482 together with the observation that during the light phase the decreased power in the gamma bands
483 was still present at a time of day when LMA did not significantly differ, argue against an association
484 between the decreased power in the gamma bands of *Cirbp* KO mice and their increased LMA.

485 Interestingly, gamma oscillations are associated with a palette of cognitive processes [reviewed
486 in (Bosman et al., 2014)]. This is further supported by associations between behavioral impairments
487 and changes in gamma power. For example, mice with abnormal interneurons are impaired at the
488 behavioral level (*e.g.* lack of cognitive flexibility) and have a reduction in task-evoked gamma power
489 in their EEG. Pharmacological stimulation of inhibitory GABA-neurons augmented power in the
490 gamma band and rescued the behavioral phenotype of the mutants (Cho et al., 2015).

491 In the hippocampus, gamma-theta coupling, *i.e.* the occurrence of gamma oscillations at a
492 specific phase of the theta oscillation, has been suggested to aid processes underlying memory [for
493 review see (Colgin, 2015)]. Because CIRBP slows down TPF and increases power in the gamma
494 bands, further analyses and experiments can address if *Cirbp* KO mice have altered phase coherence
495 between these two frequency bands. Together with the postulated function of gamma power in
496 cognitive flexibility, it would be interesting to assess if the spectral phenotype in *Cirbp* KO mice is
497 associated with behavioral abnormalities.

498 Several aspects of waking that appeared to differ between *Cirbp* KO and WT mice under baseline
499 dark conditions but were non-significant, reached significance during the recovery dark phase. For
500 example, during baseline *Cirbp* KO mice were 4% more awake and 13% more in TDW compared to
501 their WT littermates, which was amplified to 8% and 20%, respectively, during recovery. Also, TPF
502 and the genotype-dependent association between overall TPF and LMA reached significance during
503 the recovery. This suggest that SD amplified the genotypic differences. Other sleep deprivation
504 studies found evidence for similar phenomena, where sleep disturbance can amplify molecular and
505 behavioral phenotypes of Alzheimers' mouse models (for review, see (Musiek and Holtzman, 2016))
506 and sensitivity to pain (Sutton and Opp, 2014). Our data indicates that a similar phenomenon
507 occurs in *Cirbp* KO mice, where a single 6-hr SD reveals the suggestive baseline genotypic
508 differences. It would be interesting to understand the dynamics of this change; *e.g.* if they are
509 reversible or if a second SD could augment genotypic differences further.
510
511
512

513 CIRBP ADJUSTS CLOCK GENE EXPRESSION AND REM SLEEP RECOVERY FOLLOWING SD

514 CIRBP modulated the cortical response to SD in the expression of three out of the five clock
515 genes quantified. As anticipated, the SD incurred decrease in cortical *Rev-erbα* was attenuated in
516 *Cirbp* KO mice. REV-ERBα acts as a transcriptional repressor of positive clock elements such as
517 BMAL1 (Preitner et al., 2002). Mice lacking both *Rev-erbα* and its homolog *Rev-erbβ* have a shorter
518 and unstable period under constant conditions and deregulated lipid metabolism (Cho et al., 2012).
519 We recently established that *Rev-erbα* also partakes in several aspects of sleep homeostasis: *Rev-*
520 *erbα* KO mice accumulate at a slower rate NREM sleep need and have reduced efficiency of REM
521 sleep recovery in the first hours after SD (Mang et al., 2016).

522 The expression of the clock genes *Per2* and *Clock* was also modulated in the absence of CIRBP,
523 suggesting that parts of the core clock are sensitive to the presence of CIRBP in response to SD.
524 Given the role of clock genes in sleep homeostasis (Franken, 2013), the modulated clock gene
525 expression in KO mice could have contributed to the REM homeostatic sleep phenotype. This is
526 supported by studies showing that mutations in clock genes incurred a loss in REM sleep recovery
527 [*i.e.* CLOCK (Naylor et al., 2000)], or impacted the initial efficiency of REM sleep recovery [*i.e.* DBP
528 (Franken et al., 2000), PER3 (Hasan et al., 2011), and REV-ERBα (Mang et al., 2016). Follow-up
529 studies can address if indeed the changes in clock gene expression in *Cirbp* KO mice are functionally
530 implicated in the REM sleep phenotype.

531 The other aspects of the homeostatic regulation of sleep that we inspected, NREM EEG delta
532 power and time spent in NREM sleep after sleep deprivation, were unaffected in *Cirbp* KO mice.
533 Thus, CIRBP participates specifically in REM sleep homeostasis, whereas we do not find evidence
534 for its participation in NREM sleep homeostatic mechanisms.

535

536 OTHER MECHANISMS LINKING SLEEP-WAKE STATE TO CLOCK GENE EXPRESSION

537 Our results show that other pathways besides CIRBP must contribute to the sleep-wake driven
538 changes in clock gene expression. Some suggestions for such pathways are shortly discussed below,
539 as well considerations that could potentially account for the absence of a more widespread CIRBP
540 dependent change in clock gene expression that we expected based on *in vitro* results.

541 *Rbm3* (RNA Binding Motif Protein 3), another cold-inducible transcript which is closely related
542 to CIRBP, also conveys temperature information into high amplitude clock gene expression *in vitro*
543 (Liu et al., 2013). Like *Cirbp*, its expression is sleep-wake driven (Wang et al., 2010). Thus, RBM3
544 might be another mechanism through which changes in sleep-wake state are linked to changes in

545 clock gene expression and could therefore also explain the absence of a widespread CIRBP
546 dependent SD-incurred change in clock gene expression. A follow-up study could address this
547 possibility by quantifying the SD-evoked changes in clock gene expression in double *Cirbp-Rbm3*
548 KO mice.

549 Heat shock factor 1 (*Hsf1*) is a member of the heat shock pathway and *in vitro* studies showed
550 that it conveys temperature information to the circadian clock by initiating *Per2* transcription
551 through binding to *Per2*'s upstream heat shock elements (Tamaru et al., 2011). Under undisturbed
552 conditions, both *Hsf1* mRNA and protein levels are constitutively expressed, but the protein exhibits
553 daily re-localization during the dark phase to the nucleus where it acts as a transcription factor
554 (Reinke et al., 2008). Interestingly, CIRBP binds to the 3'UTR of *Hsf1* transcript [(Morf et al., 2012),
555 see supplementary data therein], although it is unclear if this affects the transcriptional activity of
556 HSF1. We found that SD induced a significant increase in *Hsf1* only in KO mice, which is congruent
557 with the observation that the expression of two other transcripts downstream of HSF1, *Hsp90b* and
558 *Hspa5/BiP*, was significantly amplified in KO mice after SD. Altogether, this suggests that the
559 increased expression of *Per2* in KO mice might be linked to increased *Hsf1* expression, and
560 underscores the presence of other temperature (and thus sleep-wake) driven pathways that can
561 ultimately affect clock gene expression.

562 Beyond temperature, many other physiological changes occur during wakefulness that can
563 subsequently affect clock gene expression. For example, oxygen consumption changes with sleep-
564 wake state (Jung et al., 2011) and oxygen levels can modulate the expression of clock genes through
565 HIF1α (Adamovich et al., 2017). Moreover, during SD, corticosterone levels increase which
566 subsequently amplifies the expression of some, but not all, clock genes (Mongrain et al., 2010).

567 Another factor to consider is that the SD-incurred changes in clock gene expression depend also
568 on an intact clock gene circuitry. For example, *Npas2* KO mice showed a reduced increase in *Per2*
569 expression in the forebrain after SD (Franken et al., 2006), while *Cry1,2* double-KO mice display a
570 larger increase in *Per2* expression after SD (Wisor et al., 2008). Thus, differences in clock gene
571 circuitry, as suggested by the *in vitro* data (Liu et al., 2013, Morf et al., 2012), could also have
572 contributed to the observed changes in clock gene expression after SD in *Cirbp* KO.

573 We could not corroborate the hepatic increase in heat shock transcripts (*Hsf1*, *Hsp90b* and
574 *Hspa5*) and in *Per2* after SD as reported in other studies (Diessler et al., 2018, Maret et al., 2007),
575 whereas we did confirm the SD-induced changes in *Cirbp*, *Rbm3-short*, *Dbp* and *Rev-erbα*. We
576 cannot readily explain this lack of confirmation.

577 Finally, we would like to briefly address an obvious shortcoming. The hypothesis of this study
578 is based on results obtained in a relatively simple biological model (*i.e.*, immortalized fibroblasts)
579 and applied to a much more complex model (*i.e.*, cortices and livers of male mice). Unpublished
580 observations on the circadian dynamics of the expression of CLOCK-BMAL1 target genes in the
581 liver, such as *Rev-erbα* and *Dbp*, show an increased circadian amplitude in *Cirbp* KO mice; *i.e.* the
582 opposite phenotype from that observed *in vitro* (Schibler et al., 2015). Along those lines, we could
583 not consistently reproduce the importance of CIRBP in determining the *ext/com* ratio of *Sfpq* (see
584 also Figure 4-B). Thus, *in vitro* findings will not always predict *in vivo* results, which could account
585 for the lack of a widespread CIRBP-dependent change in clock gene expression after SD.
586
587 CONCLUSION
588 This hypothesis-driven study explored whether the SD-induced changes in clock gene
589 expression could be mediated through the cold-induced transcript CIRBP. After SD, the cortical
590 expression of *Rev-erbα*, which we recently identified as a player in the sleep homeostat (Mang et
591 al., 2016), was attenuated in *Cirbp* KO mice, whereas the expression of two other clock genes, *Per2*
592 and *Clock*, was amplified. Thus, the SD induced changes in clock gene expression are, in part,
593 modulated by CIRBP.
594 A large body of evidence has shown that clock genes are crucial for metabolism (reviewed in
595 (Panda, 2016)). This is supported by the observation that disturbance of clock gene expression,
596 through for example genetic manipulations in mice or shift work in humans, can lead to the
597 development of metabolic disorders (Rudic et al., 2004) (Karlsson et al., 2001). Not only sleeping at
598 the wrong time, but also sleeping too little or of poor quality can induce disturbed metabolic state
599 both in rats (Barf et al., 2010) and humans (Copinschi et al., 2014). Because sleep loss affects clock
600 gene expression (Franken, 2013), we propose that this could represent a common pathway through
601 which both sleep and circadian disturbances lead to metabolic pathologies. It is thus of importance
602 to determine the pathways through which a disturbed sleep-wake distribution affects clock gene
603 expression. We show that temperature and CIRBP partake in this process, and we identified the
604 expression of *Rev-erbα* as one of the genes affected by CIRBP. Genetic (Delezie et al., 2012) and
605 pharmacological (Solt et al., 2012) studies have shown that this transcriptional repressor is
606 important for healthy metabolic functioning. Further experiments could address the metabolic
607 consequences of the attenuated response in *Rev-erbα* to sleep loss.
608

Acknowledgements

We would like to thank Maxime Jan for his help in constructing the linear mixed model, our colleagues for their assistance with the sleep deprivations, Hannes Richter from the Genomic Technology Facility, for his support when setting up the RT-qPCR, David Gatfield and Bulak Arpat for fueling insightful discussions, and Jun Fujita (Kyoto University, Japan) for sharing the *Cirbp* KO mice. This study was performed at the University of Lausanne, Switzerland, and supported by the Swiss National Science Foundation (SNF n°146694 to PF supporting MMBH) and the state of Vaud (supporting MMBH, YE and PF).

Material and Methods

MICE AND HOUSING CONDITIONS

Cirbp KO mice, kindly provided by Prof Jun Fujita (Kyoto University, Japan), were maintained on a C57BL6/J background. In these mice, *Cirbp* exons were replaced by a TK-neo gene through homologous recombination in D3 embryonic stem cells, resulting in the absence of the *Cirbp* transcript and protein (Masuda et al., 2012). Breeding couples or trios consisted of heterozygous male and female mice. WT littermates were used as controls. Throughout all the experiments, mice were individually housed in polycarbonate cages (31×18×18 cm) with food and water *ad libitum* and exposed to a 12 h light/12 h dark cycle (70–90 lux). All experiments were approved by the Ethical Committee of the State of Vaud Veterinary Office Switzerland under license VD2743 and 3201.

EEG/EMG AND THERMISTOR SURGERY

At the age of 9 to 13 weeks, 17 KO and 20 WT male mice were implanted with electroencephalogram (EEG) and electromyogram (EMG) electrodes (8 experimental cohorts).The surgery took place under deep xylazine/ ketamine anesthesia supplemented with isoflurane (1%) when necessary; for details see (Mang and Franken, 2012). Briefly, six gold-plated screws (diameter 1.1 mm) were screwed bilaterally into the skull over the frontal and parietal cortices. Two screws served as EEG electrodes and the remaining four anchored the electrode connector assembly to the skull. As EMG electrodes, two gold wires were inserted into the neck musculature. Of all EEG/EMG implanted mice, 8 KO and 9 WT mice were additionally implanted with a thermistor (serie P20AAA102M, General Electrics (currently Thermometrics), Northridge, California, USA) which was placed on top of the right cortex (2.5 mm lateral to the midline, 2.5 mm posterior to bregma). The EEG and EMG electrodes and thermistor were soldered to a connector and cemented to the skull. Mice recovered from surgery during 5–7 days before they were connected to the recording cables in their home cage for habituation, which was at least 6 days prior to the experiment. In total no less than 11 days were scheduled between surgery and start of experiment.

EXPERIMENTAL PROTOCOL AND DATA ACQUISITION

EEG and EMG signals, T_{cx} and LMA were recorded continuously for 96 h. The recording started at light onset; i.e., Zeitgeber Time (ZT)0. During the first 48 h (days BL1 and BL2), mice were left undisturbed to establish a baseline. Starting at ZT0 of day 3, mice were sleep deprived by gentle handling for 6 hours (ZT0–6), as described in (Mang and Franken, 2012). The remaining 18 h of day

3 and the entire day 4 were considered as recovery (days REC1 and REC2, respectively). The analog EEG and EMG signals were amplified (2,000×), digitized at 2 kHz and subsequently down sampled to 200 Hz and stored. The EEG was subjected to a discrete Fourier transformation yielding power spectra (range: 0–100 Hz; frequency resolution: 0.25 Hz; time resolution: consecutive 4-sec epochs; window function: Hamming). Thermistors were supplied with a constant measuring current (I_{const} = 100 microA), and voltage (V) was measured at 10 Hz to calculate the median resistance (R_t) per 4-s epoch as in eq. (1).

$$(1)\ \mathrm{R_t} = \frac{V}{\mathrm{I_{const}}}$$

Each thermistor has an individual material constant, β. The resistance was measured at 25°C ($R_{25°C}$) and 37°C ($R_{37°C}$) by the manufacturer, and used to determine β as in eq.(2), with T values in Kelvin (°C + 273.15).

$$(2)\ \beta = \frac{T_{25} * T_{37}}{T_{25} - T_{37}} * \ln \frac{R_{37°C}}{R_{25°C}}$$

Following on eq. (2), the temperature (t) in °C can be calculated as described in eq. (3).

$$(3)\ \ t(°\mathrm{C}) = \left[\frac{1}{\beta} * \log\left[\frac{R_t}{R_{25°C}}\right] + \frac{1}{T_{25°C}}\right]^{-1} - 273.15$$

The EEG, EMG, and voltage across the thermistor were recorded with Hardware (EMBLA) and software (Somnologica-3) purchased from Medcare Flaga (EMBLA, ResMed, USA). LMA was detected with passive infrared sensors (Visonic Ltd, Tel Aviv, Israel) and quantified with ClockLab software (ClockLab, ActiMetrics, Wilmette, Illinois, USA).

ANALYSIS OF LMA

To inspect the time course of LMA corrected for time-spent-awake, raw LMA was expressed per unit of waking in percentiles to which an equal amount of time-spent-awake contributed (as in Figure 3-G). The number of percentiles per recording period were chosen according to the prevalence of wakefulness, where 6 percentiles were used during the light phase and 12 during the dark phase, with the exception for 6 sections during the SD and 3 sections during the remaining 6hrs of the light phase of REC1. To assess genotype differences in LMA (Figure 6), the absolute number of movements were inspected. The LMA recordings of four mice (3 WT, 1 KO) were interrupted due to technical problems during the experiment, leaving data from 17 WT and 16 KO mice for analyses involving LMA.

681 We determined in 5 WT and 7 KO mice after the EEG-based sleep phenotyping their circadian
682 period under at least two weeks of constant darkness. Period length was determined by Chi-squared
683 test with ClockLab software (ClockLab, ActiMetrics, Wilmette, Illinois, USA).
684
685 DETERMINATION OF BEHAVIORAL STATES
686 Offline, the mouse's behavior was visually classified as 'Wakefulness', 'REM sleep', or 'NREM
687 sleep' for consecutive 4-sec epochs based on the EEG and EMG signals, as previously described
688 (Mang and Franken, 2012). Wakefulness was characterized by EEG activity of mixed frequency and
689 low amplitude and variable muscle tone. NREM sleep was defined by synchronous activity in the
690 delta frequency range (1–4 Hz), and low and stable muscle tone. REM sleep was characterized by
691 regular theta oscillations (6–9 Hz) with low EMG activity. Waking was further differentiated into
692 'quiet waking' and 'theta-dominated waking' (TDW). TDW was determined based on the relative
693 importance of power in the 6.5 to 12.0 Hz range to the overall power in the EEG of an artefact-free
694 epoch scored as wakefulness, as described in (Vassalli and Franken, 2017). We refer to waking that
695 is not classified as TDW as 'quiet' waking. Epochs containing EEG artefacts were marked according
696 to the state in which they occurred and excluded from EEG spectral analysis but included in the
697 sleep-wake distribution analyses. During the four day recording, 7.0 ± 0.9%, 2.1 ± 0.3% and 2.5 ±
698 0.2% of the epochs were scored as an artefact in waking, NREM, and REM sleep, respectively, and
699 this did not differ between genotypes (t-tests, $t(35)=1.77$, $p=0.09$; $t(35)=0.64$, $p=0.53$; $t(35)= 0.99$,
700 $p=0.33$, respectively).
701
702 ANALYSIS OF CORTICAL TEMPERATURE
703 The raw T_{cx} data showed unexpected variation. Therefore, we inspected the inter-individual
704 variation in daily amplitude and absolute T_{cx} levels. The latter was determined in two ways: i) by
705 averaging T_{cx} during the last five hours of SD, thus minimizing the sleep-wake state incurred
706 differences in T_{cx}, and ii) by averaging T_{cx} during the 12h baseline light phase. These measures were
707 highly correlated ($R^2=0.99$; $p<0.0001$). Variation in the daily amplitude was quantified by averaging
708 the difference between the highest and lowest hourly mean of T_{cx} of each of the two baseline days.
709 No effect of genotype on absolute average T_{cx} or amplitude was detected (t-test, $t(12)=0.61$, $p=0.55$;
710 $t(12)=-0.63$, $p=0.54$, respectively). Two mice (one of each genotype) exhibited a ca. 2-fold reduction
711 in amplitude together with 2°C higher values during the SD relative to the other mice (Figure 7,
712 pink symbols). Therefore, we excluded these two mice from subsequent T_{cx} analysis. Three other

713 mice (2 WT and 1 KO) showed normal amplitude but overall lower absolute values (Figure 7, blue
714 symbols). We corrected for this difference by raising their T_{cx} values by the difference between the
715 T_{cx} reached in each of these 3 mice during the SD to the average T_{cx} reached over the same recording
716 period in the remaining 9 mice. Of note, most of our T_{cx} analysis focuses on its relative sleep-wake
717 dependent changes, which are not affected by differences in absolute T_{cx} values. Finally, the baseline
718 T_{cx} data that was used to construct Figure 2B was based on 7 WT and 7 KO mice. During the
719 recording, one KO mouse and one WT mouse had random fluctuations of T_{cx} beyond physiological
720 reach and were therefore excluded from analysis involving the daily dynamics of T_{cx} (Figure 3). In
721 the recovery, a KO mouse was excluded due to aberrant high T_{cx} that could not be accounted for
722 by the sleep-wake distribution, leaving 6 WT and 5 KO mice for analyses involving REC1 and REC2.

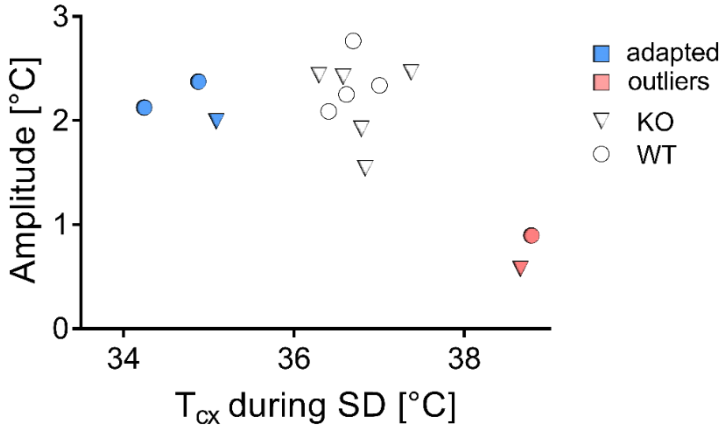

Figure 7 **Assessment of amplitude and absolute values of cortical temperatures**. Two outliers were detected (pink), whereas three others were corrected for their low values (blue).

723

724 Because visualization of all 4-s epochs occurring in 24-hour day is not compatible with the
725 resolution of Figure 2-A, sleep-wake states were averaged per minute and assigned to either wake,
726 NREM or REM sleep. Because REM sleep occurs less and in shorter bouts than waking and NREM
727 sleep, this stage is slightly underrepresented in the hypnogram of Figure 2-A. T_{cx} was averaged per
728 minute.

729 We inspected T_{cx} 1.5 min before and after sleep-wake transitions (*i.e.*, transitioning from wake
730 to NREM sleep, NREM to REM sleep, REM sleep to wake and NREM sleep to wake). A sleep-wake
731 transition was selected when the state before and after the transition lasted at least 8 epochs (*i.e.*
732 >32 sec). With this criterion, an average of 38 wake to NREM sleep, 101 NREM sleep to REM sleep,
733 28 REM sleep to wake and 32 NREM sleep to wake transitions per mouse during the two baseline
734 days was detected. The temperature profile of T_{cx} before and after the transition was constructed
735 by depicting T_{cx} relative to the mean T_{cx} at a given sleep-wake transition (*i.e.*, the average of T_{cx} in

736 the epoch before and after the sleep-wake transition). We subsequently constructed an individuals'
737 average change in T_{cx} for each sleep-wake transition. For this average, at least 10 traces were
738 contributing at a given point in time to prevent skewing of the average individual temperature
739 profile by few T_{cx} traces. Thus, the further from the sleep-wake state transition, the less epochs
740 contributed to the average individual T_{cx} profile. One WT mouse exhibited an extreme drop in T_{cx}
741 (-0.2°C in a 4-second epoch) after the transition from NREM sleep to wake in its average T_{cx} trace,
742 but not in other sleep-wake transitions. We attributed this observation to a technical artefact and
743 therefore this mouse was excluded from the NREM sleep to wake transitions.
744 The residuals of the correlation between waking and T_{cx} exhibited a circadian pattern under
745 baseline conditions. We visualized the properties of this pattern further by fitting a sinewave
746 through the data (Prism, non-linear regression; sine-wave with non-zero baseline; least squares fit).
747
748 ANALYSIS OF EEG BASED ON BEHAVIORAL STATE
749 Unless otherwise stated, all mice (20 WT and 17 KO) were included in the analyses based on the
750 EEG data. Spectral content of the EEG within sleep-wake states was calculated as follows. To
751 account for inter-individual differences in overall EEG power, EEG spectra were expressed as a
752 percentage of an individual reference value calculated as the total EEG power across 0.75-45 Hz and
753 all sleep-wake states in the 48h baseline. This reference value was weighted so that for all mice the
754 relative contribution of the three sleep-wake states (wake, NREM and REM sleep) to this reference
755 value was equal.
756 Theta peak frequency (TPF) was calculated by determining the frequency at which power
757 density peaks per 4-s epoch and subsequently averaged per individual. Power density peaks were
758 quantified from 6.5 to 12.0 Hz band and from 5.5 to 12.0 Hz band for TDW and REM sleep,
759 respectively.
760 Time course analysis of EEG delta power (*i.e.*, the mean EEG power density in the 0.75–4.0 Hz
761 range in NREM sleep) during baseline and after SD was performed as described previously (Franken
762 et al., 1999), and similar to the analysis of LMA per unit of waking. The light periods of BL1, BL2,
763 and REC2 were divided into 12 percentiles, the REC1 light period (ZT6–12) into 8 sections, and all
764 dark periods into 6 sections. The timing of these percentiles was based on the prevalence of NREM
765 sleep. EEG delta power values in NREM sleep were averaged within each percentile and then
766 expressed relative to the mean value reached in the last 4hr of the two main rest periods in baseline
767 between ZT8–12. This reference was selected because delta power reaches lowest values at this time

768 of the day and is least influenced by differences in prior history of sleep and wakefulness (see also
769 (Franken et al., 1999)). In the time course of NREM delta power, one mouse (KO) demonstrated a
770 strong decrease over the course of the experiment which could not be attributed to changes in the
771 sleep-wake distribution. 9 out of the 12 delta power values during the light phase of REC2 in this
772 mouse were outliers (MAD outlier test, consult (Leys et al., 2013) for details). This mouse was
773 excluded from the analyses involving sleep homeostasis (Figure 5).
774 The effect of 6hr SD on subsequent time spent in NREM and REM sleep was assessed by
775 calculating the recovery-baseline difference in sleep time per 1hr intervals.
776
777 SIMULATING NREM EEG DELTA POWER [PROCESS S]
778 We applied a computational method to predict the change in delta power during NREM sleep
779 based on the sleep-wake distribution as described before (Franken et al., 2001). Process S is
780 exponentially increasing with time constant τ_i during waking and REM sleep, and exponentially
781 decreasing by τ_d during NREM sleep (eq. (4) and (5), respectively).

782 $$(4)\ S_{t+1} = UA - (UA - S_t) * e^{-\frac{dt}{\tau_i}}$$

783 $$(5)\ S_{t+1} = LA + (S_t - LA) * e^{-\frac{dt}{\tau_d}}$$

784 In these simulations, UA represents the upper asymptote, LA the lower asymptote and *dt* the
785 time step of the iteration (4 seconds). Both asymptotes were estimated for each individual mouse.
786 The upper asymptote was based on the 99% level of the relative frequency distribution of delta
787 power reached in all 4s epochs scored as NREM sleep in the 4-day recording. As an estimate of the
788 lower asymptote, the intersection of the distribution of delta power values in NREM sleep with
789 REM sleep was taken. At the start of the simulation, an iteration through the first 24-hr (BL1) was
790 performed with S_0=150 at t=0. The value reached after 24-hrs is independent of S_0 at t=0 and,
791 assuming a steady state during baseline, reflects Process S at the start of the baseline for a given
792 combination of time constants.
793 The fit was optimized by minimizing the mean squared difference of simulated and observed
794 NREM delta power for a range of T_i: 1-25 h, step size 0.125h; T_d: 0.1-5.0 h, step size 0.025h; *i.e.* the
795 simulation was run for all 38'021 combinations of T_i and T_d for each mouse. The combination of T_i
796 and T_d giving the best fit was used to assess differences in process S between genotypes.
797 We noted a subtle but consistent linear discrepancy in the alignment of the simulated Process
798 S to the measured NREM delta power values at the end of the light phase on BL1, BL2 and REC2

799 (Pearson correlation, slope≠0: 1 sample t-test; t(35)=-4.38, p=0.0001). This change correlated well
800 with the day-to-day changes in total spectral power in the EEG calculated across all sleep-wake
801 states in BL1, BL2, and REC2 (Pearson correlation: R^2=0.70, p<0.0001; n=36). There was no effect of
802 genotype on slope (Δ delta power %/h; students' t-test; t(34)=0.62; p=0.54; WT:-0.086±0.027; KO:-
803 0.065±0.021) or intercept (t(34)=-0.88; p=0.38; WT: 101.5±0.62; KO: 100.7±0.56; WT: n=20, KO:
804 n=17). We attributed these linear changes to be of non-biological origin and detrended the
805 measured NREM delta power values before optimizing the fit between observed and simulated
806 delta power.
807
808 GENE EXPRESSION IN LIVER AND BRAIN
809 Five mice of each genotype (n=15 per genotype in total) were sacrificed either prior to SD (ZT0),
810 at ZT6 allowing them to sleep *ad lib* (*i.e.* without SD; ZT6-NSD), or at ZT6 after 6h SD (ZT6-SD)
811 across four experimental cohorts. Mice were randomly assigned to one of the three experimental
812 conditions. Genes of interest included transcripts affected by SD (Maret et al., 2007, Mongrain et
813 al., 2010) and/or by the presence of CIRBP (Liu et al., 2013, Morf et al., 2012) with a special interest
814 for clock genes. Specific forward and reverse primers and Taqman probes were designed
815 (seeSupplementary File 1) to quantify mRNA.
816 Upon sacrifice, both the cerebral cortex and liver were extracted and immediately flash frozen
817 in liquid nitrogen. Samples were stored at -80°C. RNA from cortex was extracted and purified using
818 the RNeasy Lipid Tissue Mini Kit 50 (QIAGEN, Hombrechtikon, Switzerland); RNA from liver was
819 extracted and purified using the RNeasy Plus Mini Kit 50 (QIAGEN, Hombrechtikon, Switzerland),
820 according to manufacturer's instructions. RNA quantity (NanoDrop ND-1000 spectrophotometer;
821 Thermo Scientific, Wilmington, NC, USA) and integrity (Fragment Analyzer, Advanced Analytical,
822 Ankeny, IA, USA) was measured and verified for each sample. 1000 ng of purified total RNA was
823 reverse-transcribed in 20µL using a mix of First-strand buffer, DTT 0.1M, random primers 0.25µg/µl,
824 dNTP 10mM, RNAzin Plus RNase Inhibitor and Superscript II reverse transcriptase (Invitrogen, Life
825 Technologies, Zug, Switzerland) according to manufacturers' procedures. The cDNA was diluted 10
826 times in Tris 10 mM pH 8.0, and 2µL of the diluted cDNA was amplified in a 10µL TaqMan reaction
827 in technical triplicates on an ABI PRISM HT 7900 detection system (Applied Biosystems, Life
828 Technologies, Zug, Switzerland). Cycler conditions were: 2 min at 50°C, 10 min at 95°C followed by
829 45 cycles at 95°C for 15 s and 60°C for 1 min. Standard curves were calculated to determine the
830 amplification efficiency (E). A sample maximization strategy was used where all biological

831 replicates of one tissue were amplified for two genes per plate. Gene expression levels were
832 normalized to two reference genes (cortex: *Eef1a* and *Gapdh*: M=0.23, CV=0.09 and liver: *Gadph* and
833 *Tbp;* M=0.32, CV=0.11) using QbasePLUS software (Biogazelle, Zwijnaarde, Belgium). *Rbm3* isoforms
834 were in a separate run quantified in liver and cortex, again with their housekeeping genes (same as
835 previously; cortex: M=0.22, and CV=0.08; liver: M=0.13, CV=0.05). Transcripts with an average Ct-
836 value>30 were omitted from analysis (in KO and WT livers: *Rbm3*, *Dusp4*, *Homer1a* and *Npas2*; in
837 cortex and liver of KO mice: *Cirbp*). Results are expressed as normalized relative quantity (NRQ)
838 which based on the overall mean expression per gene, which was set at 1.0 (Hellemans et al., 2007).

839 CIRBP affects the poly-adenylation sites of several transcripts (Liu et al., 2013). We explored if
840 this newly discovered role of CIRBP could be corroborated in our study by focusing on the transcript
841 Splicing factor, proline and glutamine rich (*Sfpq*) which exhibits CIRBP-dependent alternative poly-
842 adenylation (APA) ((Liu et al., 2013), see their Supplemental Fig4-5). We calculated the ratio of the
843 prevalence of the external 3'UTR region over the common region according to eq. (6),

844 $$(4) Ratio_{\ ext\ /\ comm} = \frac{E^{-Ct_{ext}}}{E^{-Ct_{comm}}}$$

845 where E is the amplification efficiency and Ct_{ext} and Ct_{comm} the number of cycles for the detection
846 of the extended and common isoform, respectively.

847

848 STATISTICS

849 Statistics were performed in R (version 3.3.2) and Prism (version 7.0). The threshold of
850 significance was set at p=0.05, and all statistics were solely performed on biological replicates. To
851 be more specific, our RT-qPCR data stems from 5 biological replicates, whereas amplification of
852 cDNA from one biological replicate is performed in three technical replicates. Deviations from the
853 mean are representing standard error of the mean. The distribution of the LMA data was
854 normalized by a $\log_2$ transformation on the hourly values, allowing for subsequent parametric
855 analyses on the relationship between T_{cx} and LMA as in Figure 3. Time course data were analyzed
856 by 1- and 2-way repeated measures (RM) analysis of variance (ANOVA) with as factors 'time' and
857 'genotype' (GT). Upon significance, post-hoc Fisher LSD tests were computed. Differences between
858 BL and REC values within genotype were computed by paired t-tests. EEG spectra were also
859 analyzed by 1- and 2-way RM ANOVA with as factors 'time' or 'frequency' and 'GT'. When GT or its
860 interaction with time or frequency reached significance, post-hoc t-tests were computed. The
861 above-mentioned analyses were all performed in Prism. Missing values in the sleep-wake transition

862 data of Figure 2-B led to exclusion of all data further away from the transition to perform a RM
863 ANOVA.

864 Correlation coefficients of linear regression were calculated in Prism over all hourly values of
865 LMA, T_{cx} and waking per genotype (96 per mice). To compare slopes of regression lines between
866 genotypes, an ANCOVA was applied based on (Zar, 1984) and run in Prism. To quantify the
867 contribution of waking and LMA independent from each other to T_{cx}, a partial correlation was
868 performed (R software; package 'ppcor', function pcor.test). Mixed model analysis was performed
869 with factors LMA ($\log_2$ transformed), waking, and genotype (R packages 'lme4', 'lmer', 'lmerTest',
870 and 'MuMIn'). Model1 quantified the predictive power of waking, Model2 of waking and LMA per
871 unit of waking (LMA/Waking) and Model3 of waking, LMA/Waking and its interaction, to predict
872 T_{cx}. Predictive power of models was compared with Chi-squared tests by assessing the statistical
873 significance in the reduction of residual sum of squares between two models ordered by complexity;
874 *i.e.* Model1 was compared to Model2, and upon significance, Model2 was compared to Model3.
875 Goodness-of-fit was assessed by the marginal R-squared (R^2_m) which explains the effect of the fixed
876 factors only, and the conditional R-squared (R^2_c), which considers the individual variance as well
877 and is therefore more biological relevant. Hence, in the results section only the R^2_c values are
878 reported.

879 For the molecular data, the qPCR NRQ values were $\log_2$-transformed to normalize the
880 distribution. Genotype differences at ZT0 were tested with a t-test. The effect of SD and genotype
881 at ZT6 was assessed by 2-way ANOVA with post-hoc Fisher LSD tests upon significance. One outlier
882 (WT, cortex) in the *ext/com* ratio analyses was detected by the Grubbs outliers test ($\alpha < 0.05$) and
883 excluded.

884

885

886 **Supplementary File 1**:

887 sequences of the forward and reverse primer and probe used for the RT-qPCR

GeneName	FwdPrimer	RevPrimer	Probe
Cirbp	AGGGTTCTCCAGAGGAGGAG	CCGGCTGGCATAGTAGTCTC	CGCTTTGAGTCCCGGAGTGGG
Clock	CGAGAAAGATGGACAAGTCTACTG	TCCAGTCCTGTCGAATCTCA	TGCGCAAACATAAAGAGACCACTGCA
Dbp	CGTGGAGGTGCTTAATGACCTTT	CATGGCCTGGAATGCTTGA	AACCTGATCCCGCTGATCTCGC
Dusp4	GTTCATGGAAGCCATCGAGT	CCGCTTCTTCATCATCAGGT	TCCCGATCAGCCACCATCTGC
Eef1a	CCTGGCAAGCCCATGTGT	TCATGTCACGAACAGCAAAGC	TGAGAGCTTCTCTGACTACCCTCCACTTGGT
Gadph	TCCATGACAACTTTGGCATTG	CAGTCTTCTGGGTGGCAGTGA	AAGGGCTCATGACCACAGTCCATGC
Homer1a	GCATTGCCATTTCCACATAGG	ATGAACTTCCATATTTATCCACCTTACTT	ACA5ATT5AATT5AG5AATCATGA (*)
Hsf1	CAACAACATGGCTAGCTTCG	CTCGGTGTCATCTCTCTCAGG	TGAGCAGGGTGGCCTGGTCA
Hsp90b1	TGTACCCACATCTGCACCTC	TTGGGCATCATATCATGGAA	CGCCGCGTATTCATCACAGATGA
Hspa5/Bip	CACTTGGAATGACCCTTCG	GTTTGCCCACCTCCAATATC	TGGCAAGAACTTGATGTCCTGCTGC
Npas2	AGGAAAGGACGTCTGCTTCA	CCAAGCTATGCCTCGAAGTG	CCTGGCAACCCCGCAGTTCTTA
Per2	ATGCTCGCCATCCACAAGA	GCGGAATCGAATGGGAGAAT	ATCCTACAGGCCGGTGGACAGCC
Rbm3-long	TGATGCTGTCTTCAGGATGC	GGCCCAACACAAGTAAAGGA	TCAAGGATGAGGTAAGTATGCTATCCTTGAGC
Rbm3-short	GGCTATGACCGCTACTCAGG	CAGCAATTTGCAAGGACGAT	TGAGATGGGGCATGCACACA
Nr1d1 / Rev-erbα	AGGGCACAAGCAACATTACC	CAGGCGTGCACTCCATAGT	AGGCCACGTCCCCACACACC
Sfpq	GCATTTGAAAGATGCAGTGAA	CAGGAAGACCATCTTCGTCA	TCGCCCAGTCATTGTGGAACCA
Sfpq_Comm	TGGATGTTAGCAGTTTATTGACC	GCACAAGGTACACTGCCATT	TGTAAATGGCCTGTTTGGGCAGG
Sfpq_Ext	TGCTTTCCTCCCACCATAAG	TTGCTCTAACGAAAGGAAATTCA	TGGGGATGTTTTGATGATGTCAGTTCA
Sirt1	TTGTGAAGCTGTTCGTGGAG	CTCATCAGCTGGGCACCTA	TTTTAATCAGGTAGTTCCTCGGTGCCC
Tbp	TTGACCTAAAGACCATTGCACTTC	TTCTCATGATGACTGCAGCAAA	TGCAAGAAATGCTGAATATAATCCCAAGCG

888

889

890

891 (*) 5 = propynyl-dC ; increases the melting temperature of the probe

892

References

ADAMOVICH, Y., LADEUIX, B., GOLIK, M., KOENERS, M. P. & ASHER, G. 2017. Rhythmic Oxygen Levels Reset Circadian Clocks through HIF1alpha. *Cell Metab,* 25**,** 93-101.

ALFOLDI, P., RUBICSEK, G., CSERNI, G. & OBAL, F., JR. 1990. Brain and core temperatures and peripheral vasomotion during sleep and wakefulness at various ambient temperatures in the rat. *Pflugers Arch,* 417**,** 336-41.

ARCHER, S. N., LAING, E. E., MOLLER-LEVET, C. S., VAN DER VEEN, D. R., BUCCA, G., LAZAR, A. S., SANTHI, N., SLAK, A., KABILJO, R., VON SCHANTZ, M., SMITH, C. P. & DIJK, D. J. 2014. Mistimed sleep disrupts circadian regulation of the human transcriptome. *Proc Natl Acad Sci U S A,* 111**,** E682-91.

BAKER, F. C., ANGARA, C., SZYMUSIAK, R. & MCGINTY, D. 2005. Persistence of sleep-temperature coupling after suprachiasmatic nuclei lesions in rats. *Am J Physiol Regul Integr Comp Physiol,* 289**,** R827-38.

BAKER, M. A. & HAYWARD, J. N. 1968. The influence of the nasal mucosa and the carotid rete upon hypothalamic temperature in sheep. *J Physiol,* 198**,** 561-79.

BARF, R. P., MEERLO, P. & SCHEURINK, A. J. 2010. Chronic sleep disturbance impairs glucose homeostasis in rats. *Int J Endocrinol,* 2010**,** 819414.

BOSMAN, C. A., LANSINK, C. S. & PENNARTZ, C. M. 2014. Functions of gamma-band synchronization in cognition: from single circuits to functional diversity across cortical and subcortical systems. *Eur J Neurosci,* 39**,** 1982-99.

BUZSÁKI, G. 2006. *Rhythms of the brain,* England, Oxford University Press.

CAMBRAS, T., WELLER, J. R., ANGLES-PUJORAS, M., LEE, M. L., CHRISTOPHER, A., DIEZ-NOGUERA, A., KRUEGER, J. M. & DE LA IGLESIA, H. O. 2007. Circadian desynchronization of core body temperature and sleep stages in the rat. *Proc Natl Acad Sci U S A,* 104**,** 7634-9.

CHO, H., ZHAO, X., HATORI, M., YU, R. T., BARISH, G. D., LAM, M. T., CHONG, L. W., DITACCHIO, L., ATKINS, A. R., GLASS, C. K., LIDDLE, C., AUWERX, J., DOWNES, M., PANDA, S. & EVANS, R. M. 2012. Regulation of circadian behaviour and metabolism by REV-ERB-alpha and REV-ERB-beta. *Nature,* 485**,** 123-7.

CHO, K. K., HOCH, R., LEE, A. T., PATEL, T., RUBENSTEIN, J. L. & SOHAL, V. S. 2015. Gamma rhythms link prefrontal interneuron dysfunction with cognitive inflexibility in Dlx5/6(+/-) mice. *Neuron,* 85**,** 1332-43.

COLGIN, L. L. 2015. Theta-gamma coupling in the entorhinal-hippocampal system. *Curr Opin Neurobiol,* 31**,** 45-50.

COPINSCHI, G., LEPROULT, R. & SPIEGEL, K. 2014. The important role of sleep in metabolism. *Front Horm Res,* 42**,** 59-72.

DAAN, S., BEERSMA, D. G. & BORBELY, A. A. 1984. Timing of human sleep: recovery process gated by a circadian pacemaker. *Am J Physiol,* 246**,** R161-83.

DEBOER, T., FRANKEN, P. & TOBLER, I. 1994. Sleep and cortical temperature in the Djungarian hamster under baseline conditions and after sleep deprivation. *J Comp Physiol A,* 174**,** 145-55.

DELEZIE, J., DUMONT, S., DARDENTE, H., OUDART, H., GRECHEZ-CASSIAU, A., KLOSEN, P., TEBOUL, M., DELAUNAY, F., PEVET, P. & CHALLET, E. 2012. The nuclear receptor REV-ERBalpha is required for the daily balance of carbohydrate and lipid metabolism. *Faseb j,* 26**,** 3321-35.

DIESSLER, S., JAN, M., EMMENEGGER, Y., GUEX, N., MIDDLETON, B., SKENE, D. J., IBBERSON, M., BURDET, F., GOTZ, L., PAGNI, M., SANKAR, M., LIECHTI, R., HOR, C. N., XENARIOS, I. & FRANKEN,

P. 2018. A systems genetics resource and analysis of sleep regulation in the mouse. *PLoS Biol,* 16**,** e2005750.

DIJK, D. J. & CZEISLER, C. A. 1995. Contribution of the circadian pacemaker and the sleep homeostat to sleep propensity, sleep structure, electroencephalographic slow waves, and sleep spindle activity in humans. *J Neurosci,* 15**,** 3526-38.

DIJK, D. J., DUFFY, J. F. & CZEISLER, C. A. 2000. Contribution of circadian physiology and sleep homeostasis to age-related changes in human sleep. *Chronobiol Int,* 17**,** 285-311.

EDGAR, D. M., DEMENT, W. C. & FULLER, C. A. 1993. Effect of SCN lesions on sleep in squirrel monkeys: evidence for opponent processes in sleep-wake regulation. *J Neurosci,* 13**,** 1065-79.

FRANKEN, P. 2002. Long-term vs. short-term processes regulating REM sleep. *J Sleep Res,* 11**,** 17-28.

FRANKEN, P. 2013. A role for clock genes in sleep homeostasis. *Curr Opin Neurobiol,* 23**,** 864-72.

FRANKEN, P., CHOLLET, D. & TAFTI, M. 2001. The homeostatic regulation of sleep need is under genetic control. *J Neurosci,* 21**,** 2610-21.

FRANKEN, P., DUDLEY, C. A., ESTILL, S. J., BARAKAT, M., THOMASON, R., O'HARA, B. F. & MCKNIGHT, S. L. 2006. NPAS2 as a transcriptional regulator of non-rapid eye movement sleep: genotype and sex interactions. *Proc Natl Acad Sci U S A,* 103**,** 7118-23.

FRANKEN, P., LOPEZ-MOLINA, L., MARCACCI, L., SCHIBLER, U. & TAFTI, M. 2000. The transcription factor DBP affects circadian sleep consolidation and rhythmic EEG activity. *J Neurosci,* 20**,** 617-25.

FRANKEN, P., MALAFOSSE, A. & TAFTI, M. 1999. Genetic determinants of sleep regulation in inbred mice. *Sleep,* 22**,** 155-69.

FRANKEN, P., TOBLER, I. & BORBELY, A. A. 1992. Sleep and waking have a major effect on the 24-hr rhythm of cortical temperature in the rat. *J Biol Rhythms,* 7**,** 341-52.

FULLER, A., CARTER, R. N. & MITCHELL, D. 1998. Brain and abdominal temperatures at fatigue in rats exercising in the heat. *J Appl Physiol (1985),* 84**,** 877-83.

FURTH, K. E., MCCOY, A. J., DODGE, C., WALTERS, J. R., BUONANNO, A. & DELAVILLE, C. 2017. Neuronal correlates of ketamine and walking induced gamma oscillations in the medial prefrontal cortex and mediodorsal thalamus. *PLoS One,* 12**,** e0186732.

HASAN, S., VAN DER VEEN, D. R., WINSKY-SOMMERER, R., DIJK, D. J. & ARCHER, S. N. 2011. Altered sleep and behavioral activity phenotypes in PER3-deficient mice. *Am J Physiol Regul Integr Comp Physiol,* 301**,** R1821-30.

HAYWARD, J. N. & BAKER, M. A. 1968. Role of cerebral arterial blood in the regulation of brain temperature in the monkey. *Am J Physiol,* 215**,** 389-403.

HELLEMANS, J., MORTIER, G., DE PAEPE, A., SPELEMAN, F. & VANDESOMPELE, J. 2007. qBase relative quantification framework and software for management and automated analysis of real-time quantitative PCR data. *Genome Biol,* 8**,** R19.

HIDDINGA, A. E., BEERSMA, D. G. & VAN DEN HOOFDAKKER, R. H. 1997. Endogenous and exogenous components in the circadian variation of core body temperature in humans. *J Sleep Res,* 6**,** 156-63.

JEEWAJEE, A., BARRY, C., O'KEEFE, J. & BURGESS, N. 2008. Grid cells and theta as oscillatory interference: electrophysiological data from freely moving rats. *Hippocampus,* 18**,** 1175-85.

JUNG, C. M., MELANSON, E. L., FRYDENDALL, E. J., PERREAULT, L., ECKEL, R. H. & WRIGHT, K. P. 2011. Energy expenditure during sleep, sleep deprivation and sleep following sleep deprivation in adult humans. *J Physiol,* 589**,** 235-44.

980 KARLSSON, B., KNUTSSON, A. & LINDAHL, B. 2001. Is there an association between shift work and having
981 a metabolic syndrome? Results from a population based study of 27,485 people. *Occup Environ*
982 *Med,* 58**,** 747-52.
983 LEYS, C., LEY, C., KLEIN, O., BERNARD, P. & LICATA, L. 2013. Detecting outliers: Do not use standard
984 deviation around the mean, use absolute deviation around the median. *Journal of Experimental*
985 *Social Psychology,* 49**,** 764-766.
986 LIU, Y., HU, W., MURAKAWA, Y., YIN, J., WANG, G., LANDTHALER, M. & YAN, J. 2013. Cold-induced RNA-
987 binding proteins regulate circadian gene expression by controlling alternative polyadenylation.
988 *Sci Rep,* 3**,** 2054.
989 LOWREY, P. L. & TAKAHASHI, J. S. 2011. Genetics of circadian rhythms in Mammalian model organisms.
990 *Adv Genet,* 74**,** 175-230.
991 MANG, G. M. & FRANKEN, P. 2012. Sleep and EEG Phenotyping in Mice. *Curr Protoc Mouse Biol,* 2**,** 55-
992 74.
993 MANG, G. M. & FRANKEN, P. 2015. Genetic dissection of sleep homeostasis. *Curr Top Behav Neurosci,*
994 25**,** 25-63.
995 MANG, G. M., LA SPADA, F., EMMENEGGER, Y., CHAPPUIS, S., RIPPERGER, J. A., ALBRECHT, U. &
996 FRANKEN, P. 2016. Altered Sleep Homeostasis in Rev-erbalpha Knockout Mice. *Sleep,* 39**,** 589-
997 601.
998 MARET, S., DORSAZ, S., GURCEL, L., PRADERVAND, S., PETIT, B., PFISTER, C., HAGENBUCHLE, O., O'HARA,
999 B. F., FRANKEN, P. & TAFTI, M. 2007. Homer1a is a core brain molecular correlate of sleep loss.
1000 *Proc Natl Acad Sci U S A,* 104**,** 20090-5.
1001 MASUDA, T., ITOH, K., HIGASHITSUJI, H., HIGASHITSUJI, H., NAKAZAWA, N., SAKURAI, T., LIU, Y.,
1002 TOKUCHI, H., FUJITA, T., ZHAO, Y., NISHIYAMA, H., TANAKA, T., FUKUMOTO, M., IKAWA, M.,
1003 OKABE, M. & FUJITA, J. 2012. Cold-inducible RNA-binding protein (Cirp) interacts with
1004 Dyrk1b/Mirk and promotes proliferation of immature male germ cells in mice. *Proc Natl Acad Sci*
1005 *U S A,* 109**,** 10885-90.
1006 MONGRAIN, V., HERNANDEZ, S. A., PRADERVAND, S., DORSAZ, S., CURIE, T., HAGIWARA, G., GIP, P.,
1007 HELLER, H. C. & FRANKEN, P. 2010. Separating the contribution of glucocorticoids and
1008 wakefulness to the molecular and electrophysiological correlates of sleep homeostasis. *Sleep,*
1009 33**,** 1147-57.
1010 MORF, J., REY, G., SCHNEIDER, K., STRATMANN, M., FUJITA, J., NAEF, F. & SCHIBLER, U. 2012. Cold-
1011 inducible RNA-binding protein modulates circadian gene expression posttranscriptionally.
1012 *Science,* 338**,** 379-83.
1013 MUSIEK, E. S. & HOLTZMAN, D. M. 2016. Mechanisms linking circadian clocks, sleep, and
1014 neurodegeneration. *Science,* 354**,** 1004-1008.
1015 NAYLOR, E., BERGMANN, B. M., KRAUSKI, K., ZEE, P. C., TAKAHASHI, J. S., VITATERNA, M. H. & TUREK, F.
1016 W. 2000. The circadian clock mutation alters sleep homeostasis in the mouse. *J Neurosci,* 20**,**
1017 8138-43.
1018 NIELL, C. M. & STRYKER, M. P. 2010. Modulation of visual responses by behavioral state in mouse visual
1019 cortex. *Neuron,* 65**,** 472-9.
1020 NISHIYAMA, H., ITOH, K., KANEKO, Y., KISHISHITA, M., YOSHIDA, O. & FUJITA, J. 1997. A glycine-rich RNA-
1021 binding protein mediating cold-inducible suppression of mammalian cell growth. *J Cell Biol,* 137**,**
1022 899-908.
1023 NYBO, L., SECHER, N. H. & NIELSEN, B. 2002. Inadequate heat release from the human brain during
1024 prolonged exercise with hyperthermia. *J Physiol,* 545**,** 697-704.

1025 PANDA, S. 2016. Circadian physiology of metabolism. *Science,* 354**,** 1008-1015.
1026 PREITNER, N., DAMIOLA, F., LOPEZ-MOLINA, L., ZAKANY, J., DUBOULE, D., ALBRECHT, U. & SCHIBLER, U.
1027 2002. The orphan nuclear receptor REV-ERBalpha controls circadian transcription within the
1028 positive limb of the mammalian circadian oscillator. *Cell,* 110**,** 251-60.
1029 REINKE, H., SAINI, C., FLEURY-OLELA, F., DIBNER, C., BENJAMIN, I. J. & SCHIBLER, U. 2008. Differential
1030 display of DNA-binding proteins reveals heat-shock factor 1 as a circadian transcription factor.
1031 *Genes Dev,* 22**,** 331-45.
1032 RUDIC, R. D., MCNAMARA, P., CURTIS, A. M., BOSTON, R. C., PANDA, S., HOGENESCH, J. B. &
1033 FITZGERALD, G. A. 2004. BMAL1 and CLOCK, two essential components of the circadian clock,
1034 are involved in glucose homeostasis. *PLoS Biol,* 2**,** e377.
1035 SCHIBLER, U., GOTIC, I., SAINI, C., GOS, P., CURIE, T., EMMENEGGER, Y., SINTUREL, F., GOSSELIN, P.,
1036 GERBER, A., FLEURY-OLELA, F., RANDO, G., DEMARQUE, M. & FRANKEN, P. 2015. Clock-Talk:
1037 Interactions between Central and Peripheral Circadian Oscillators in Mammals. *Cold Spring Harb*
1038 *Symp Quant Biol,* 80**,** 223-32.
1039 SHAW, P. J., TONONI, G., GREENSPAN, R. J. & ROBINSON, D. F. 2002. Stress response genes protect
1040 against lethal effects of sleep deprivation in Drosophila. *Nature,* 417**,** 287-91.
1041 SOLT, L. A., WANG, Y., BANERJEE, S., HUGHES, T., KOJETIN, D. J., LUNDASEN, T., SHIN, Y., LIU, J.,
1042 CAMERON, M. D., NOEL, R., YOO, S. H., TAKAHASHI, J. S., BUTLER, A. A., KAMENECKA, T. M. &
1043 BURRIS, T. P. 2012. Regulation of circadian behaviour and metabolism by synthetic REV-ERB
1044 agonists. *Nature,* 485**,** 62-8.
1045 SUTTON, B. C. & OPP, M. R. 2014. Sleep fragmentation exacerbates mechanical hypersensitivity and
1046 alters subsequent sleep-wake behavior in a mouse model of musculoskeletal sensitization.
1047 *Sleep,* 37**,** 515-24.
1048 TAMARU, T., HATTORI, M., HONDA, K., BENJAMIN, I., OZAWA, T. & TAKAMATSU, K. 2011.
1049 Synchronization of circadian Per2 rhythms and HSF1-BMAL1:CLOCK interaction in mouse
1050 fibroblasts after short-term heat shock pulse. *PLoS One,* 6**,** e24521.
1051 VASSALLI, A. & FRANKEN, P. 2017. Hypocretin (orexin) is critical in sustaining theta/gamma-rich waking
1052 behaviors that drive sleep need. *Proc Natl Acad Sci U S A,* 114**,** E5464-E5473.
1053 VINCK, M., BATISTA-BRITO, R., KNOBLICH, U. & CARDIN, J. A. 2015. Arousal and locomotion make
1054 distinct contributions to cortical activity patterns and visual encoding. *Neuron,* 86**,** 740-54.
1055 VIOLA, A. U., ARCHER, S. N., JAMES, L. M., GROEGER, J. A., LO, J. C., SKENE, D. J., VON SCHANTZ, M. &
1056 DIJK, D. J. 2007. PER3 polymorphism predicts sleep structure and waking performance. *Curr Biol,*
1057 17**,** 613-8.
1058 WANG, H., LIU, Y., BRIESEMANN, M. & YAN, J. 2010. Computational analysis of gene regulation in animal
1059 sleep deprivation. *Physiol Genomics,* 42**,** 427-36.
1060 WEVER, R. A. 1979. *The Circadian System of Man,* New York, Springer-Verlag.
1061 WISOR, J. P., O'HARA, B. F., TERAO, A., SELBY, C. P., KILDUFF, T. S., SANCAR, A., EDGAR, D. M. &
1062 FRANKEN, P. 2002. A role for cryptochromes in sleep regulation. *BMC Neurosci,* 3**,** 20.
1063 WISOR, J. P., PASUMARTHI, R. K., GERASHCHENKO, D., THOMPSON, C. L., PATHAK, S., SANCAR, A.,
1064 FRANKEN, P., LEIN, E. S. & KILDUFF, T. S. 2008. Sleep deprivation effects on circadian clock gene
1065 expression in the cerebral cortex parallel electroencephalographic differences among mouse
1066 strains. *J Neurosci,* 28**,** 7193-201.
1067 ZAR, J. H. 1984. *Biostatistical Analysis* Prentice Hall.

1068 ZHENG, C., BIERI, K. W., TRETTEL, S. G. & COLGIN, L. L. 2015. The relationship between gamma frequency
1069 and running speed differs for slow and fast gamma rhythms in freely behaving rats.
1070 *Hippocampus,* 25**,** 924-38.
1071

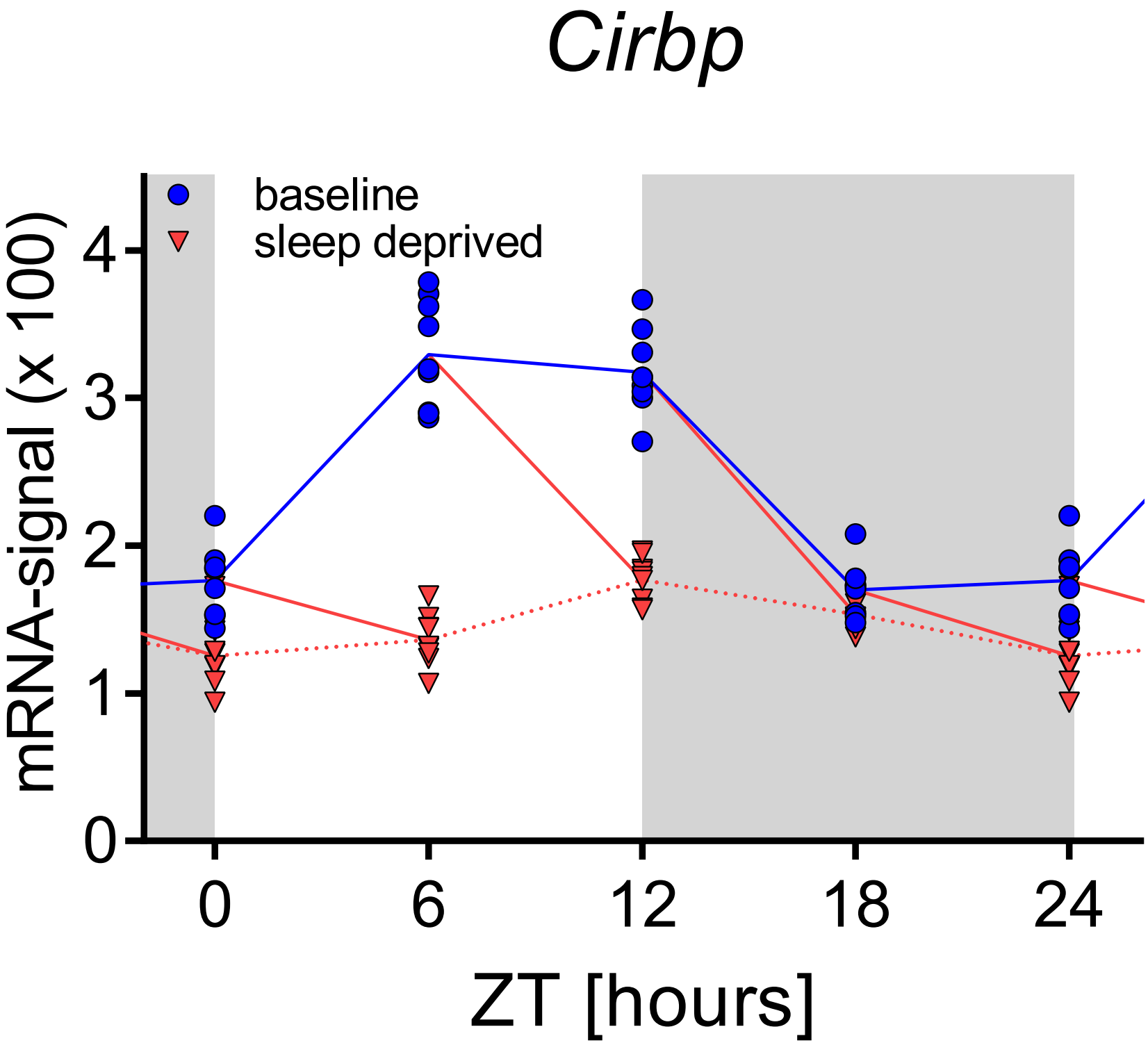
Cirbp
baseline
sleep deprived
mRNA-signal (x 100)
0
1
2
3
4
0
6
12
18
24
ZT [hours]

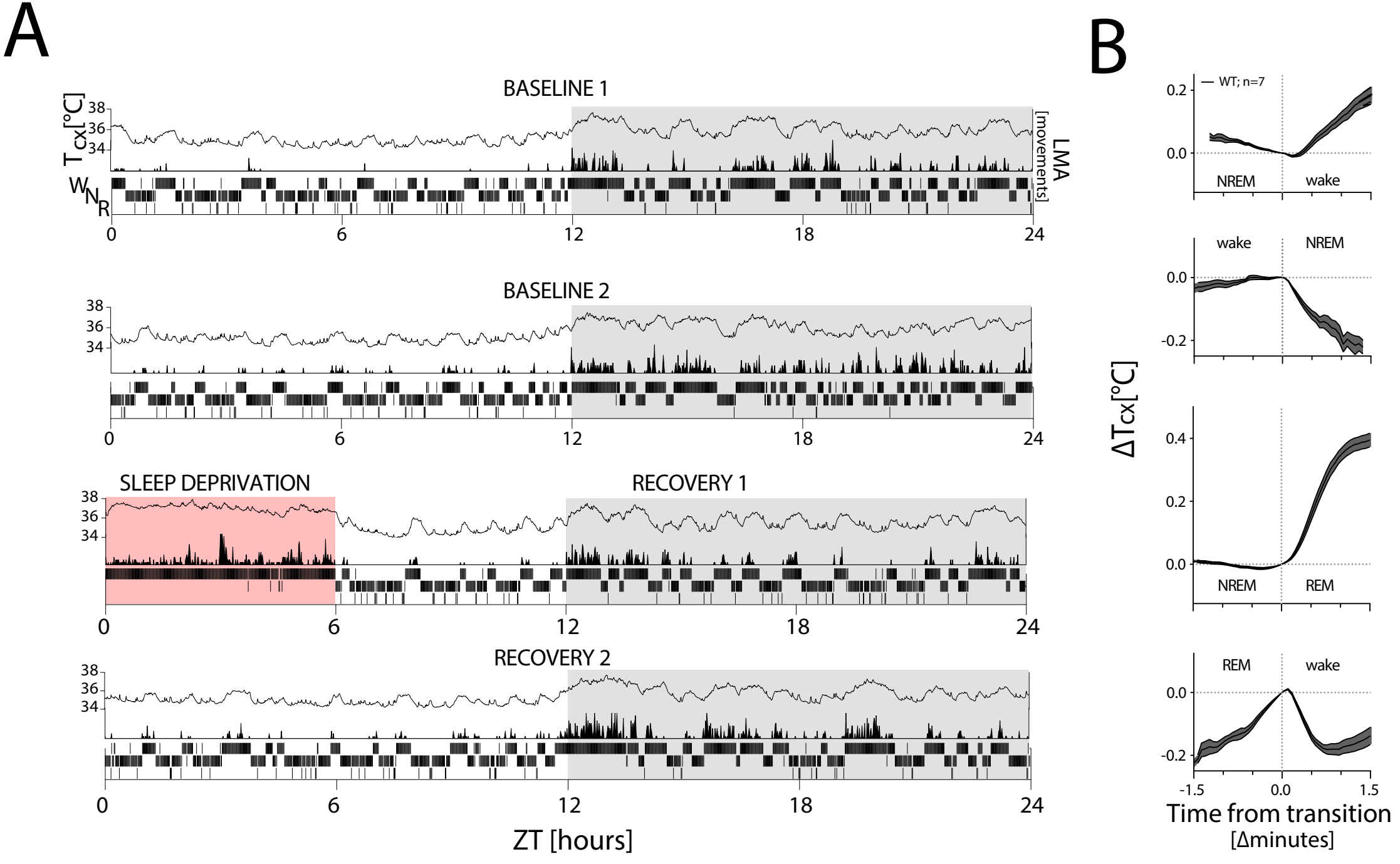
A
BASELINE 1
BASELINE 2
SLEEP DEPRIVATION
RECOVERY 1
RECOVERY 2
T cx [°C]
38
36
34
W
N
R
LMA [movements]
0
6
12
18
24
ZT [hours]
B
WT; n=7
0.2
0.0
NREM
wake
-0.2
REM
0.4
ΔTcx[°C]
-1.5
1.5
Time from transition
[Δminutes]

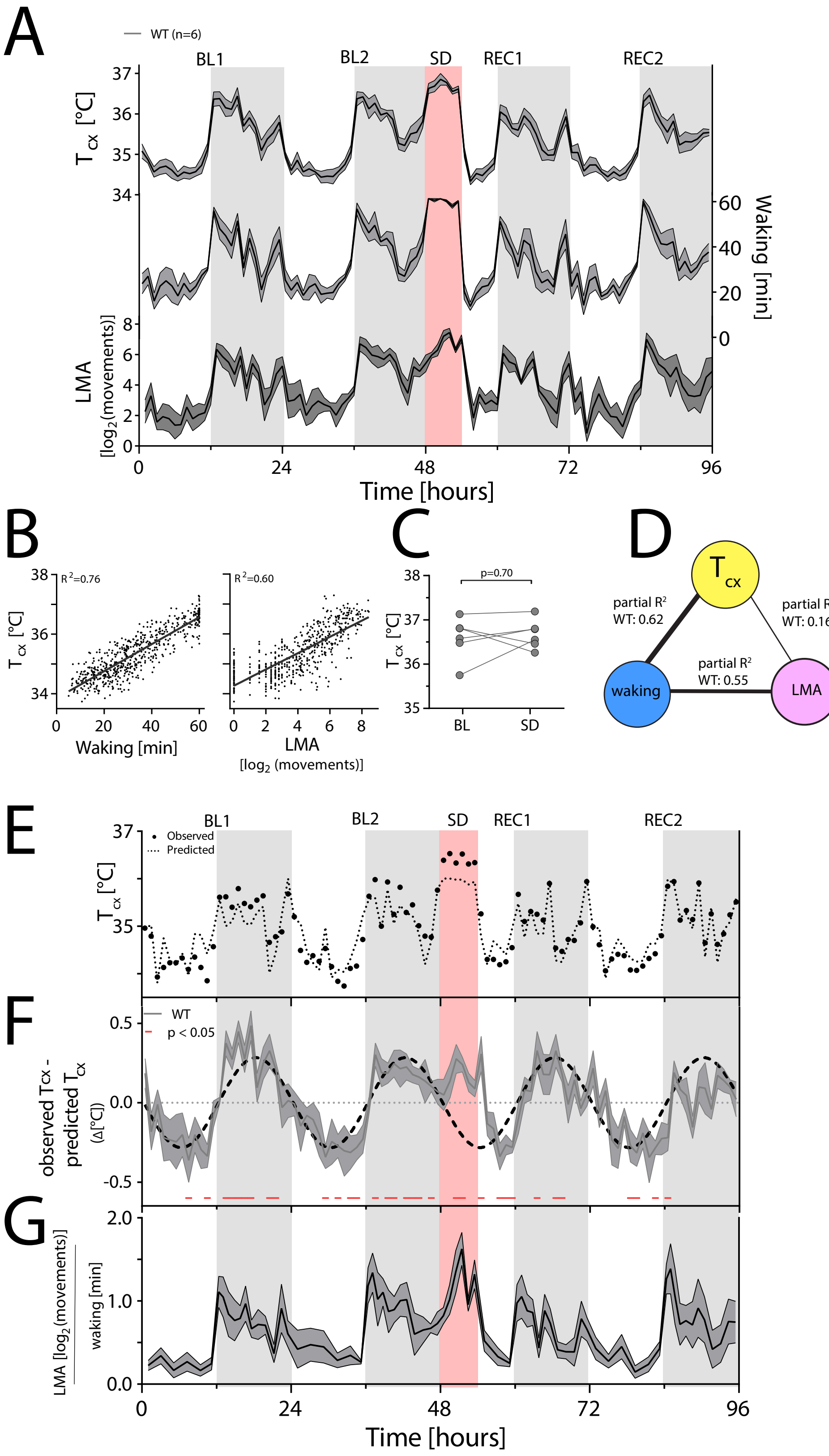
A
WT (n=6)
BL1
BL2
SD
REC1
REC2
T_{cx} [°C]
Waking [min]
LMA [$\log_2$(movements)]
Time [hours]
B
R^2=0.76
R^2=0.60
Waking [min]
LMA [$\log_2$ (movements)]
C
p=0.70
BL
SD
D
T_{cx}
partial R^2 WT: 0.62
partial R^2 WT: 0.16
partial R^2 WT: 0.55
waking
LMA
E
Observed
Predicted
F
WT
p < 0.05
observed Tcx - predicted T_{cx} (Δ[°C])
G
LMA [$\log_2$(movements)] / waking [min]

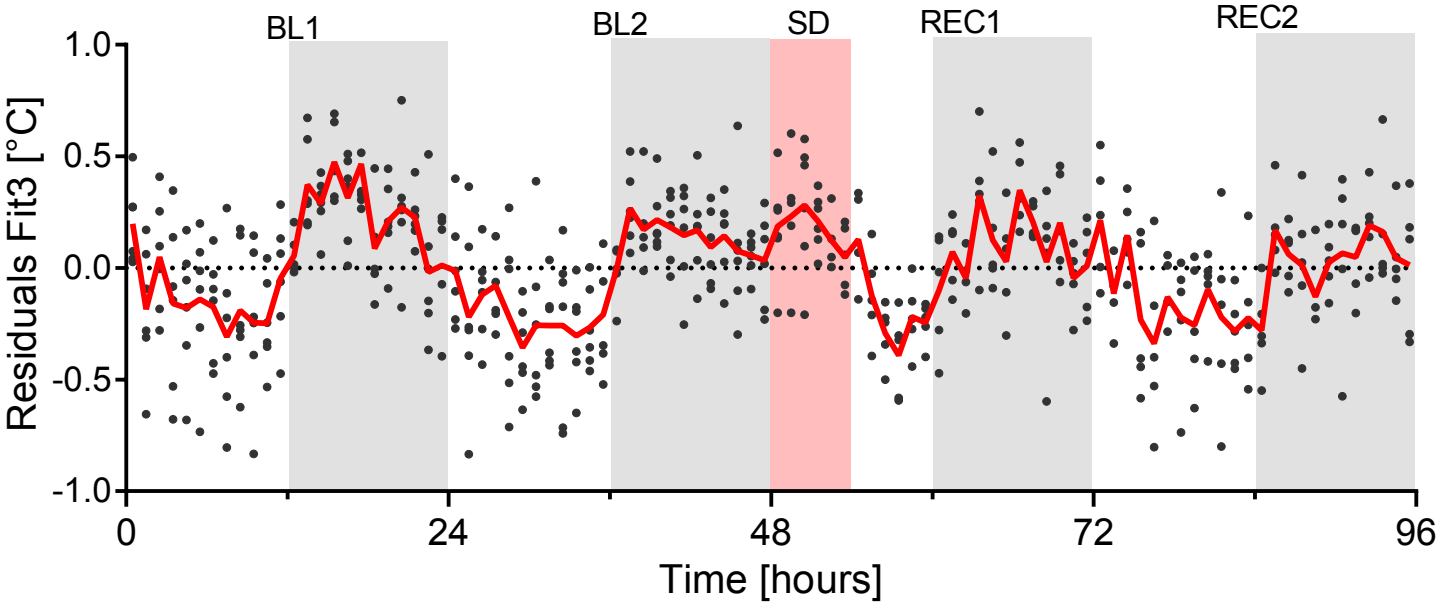
BL1
BL2
SD
REC1
REC2
1.0
0.5
0.0
-0.5
-1.0
Residuals Fit3 [°C]
0
24
48
72
96
Time [hours]

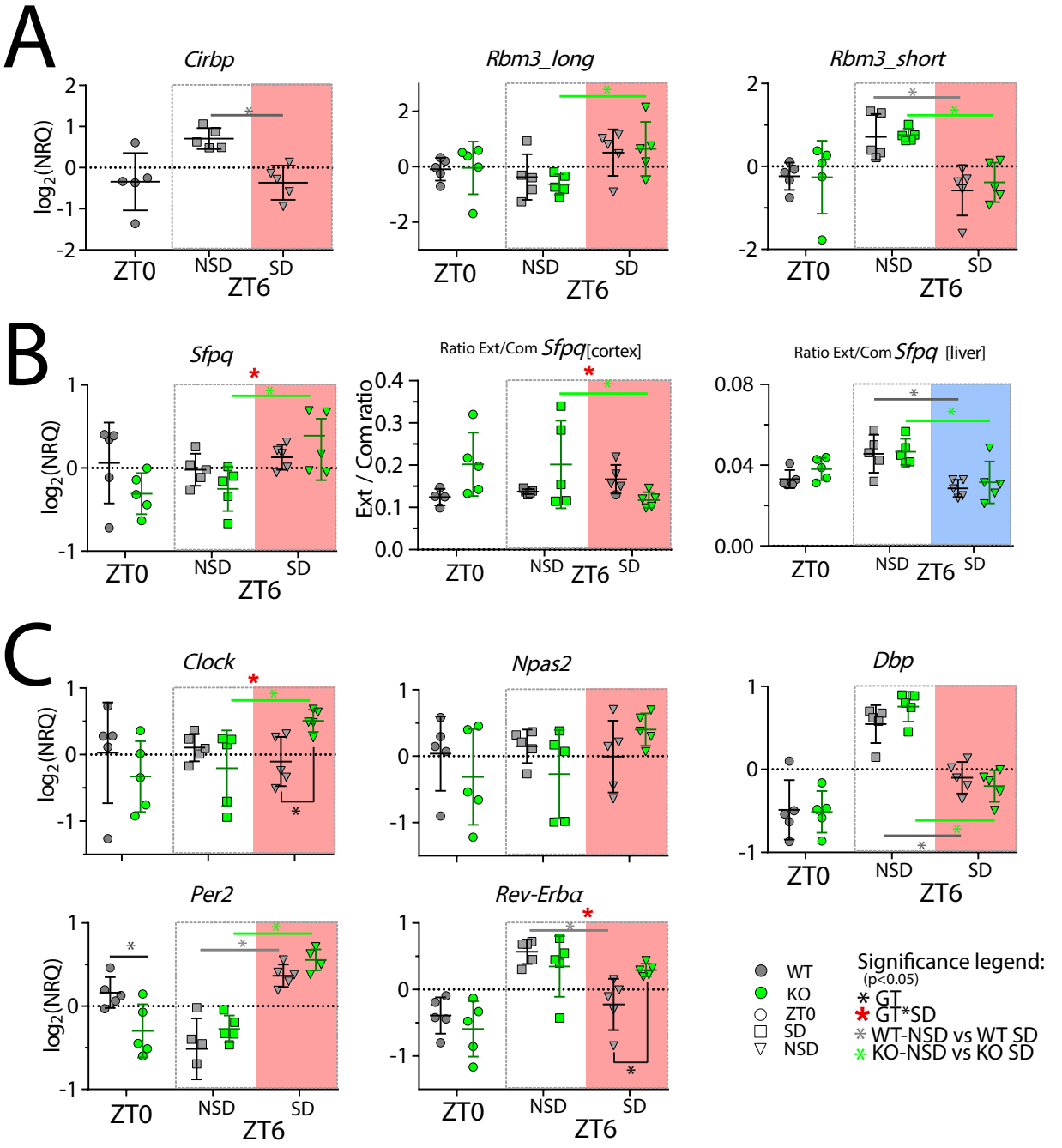
A
Cirbp
Rbm3_long
Rbm3_short
log2(NRQ)
ZT0
NSD
SD
ZT6
B
Sfpq
Ratio Ext/Com Sfpq[cortex]
Ratio Ext/Com Sfpq [liver]
Ext / Com ratio
C
Clock
Npas2
Dbp
Per2
Rev-Erbα
WT
KO
ZT0
SD
NSD
Significance legend:
(p<0.05)
* GT
* GT*SD
* WT-NSD vs WT SD
* KO-NSD vs KO SD

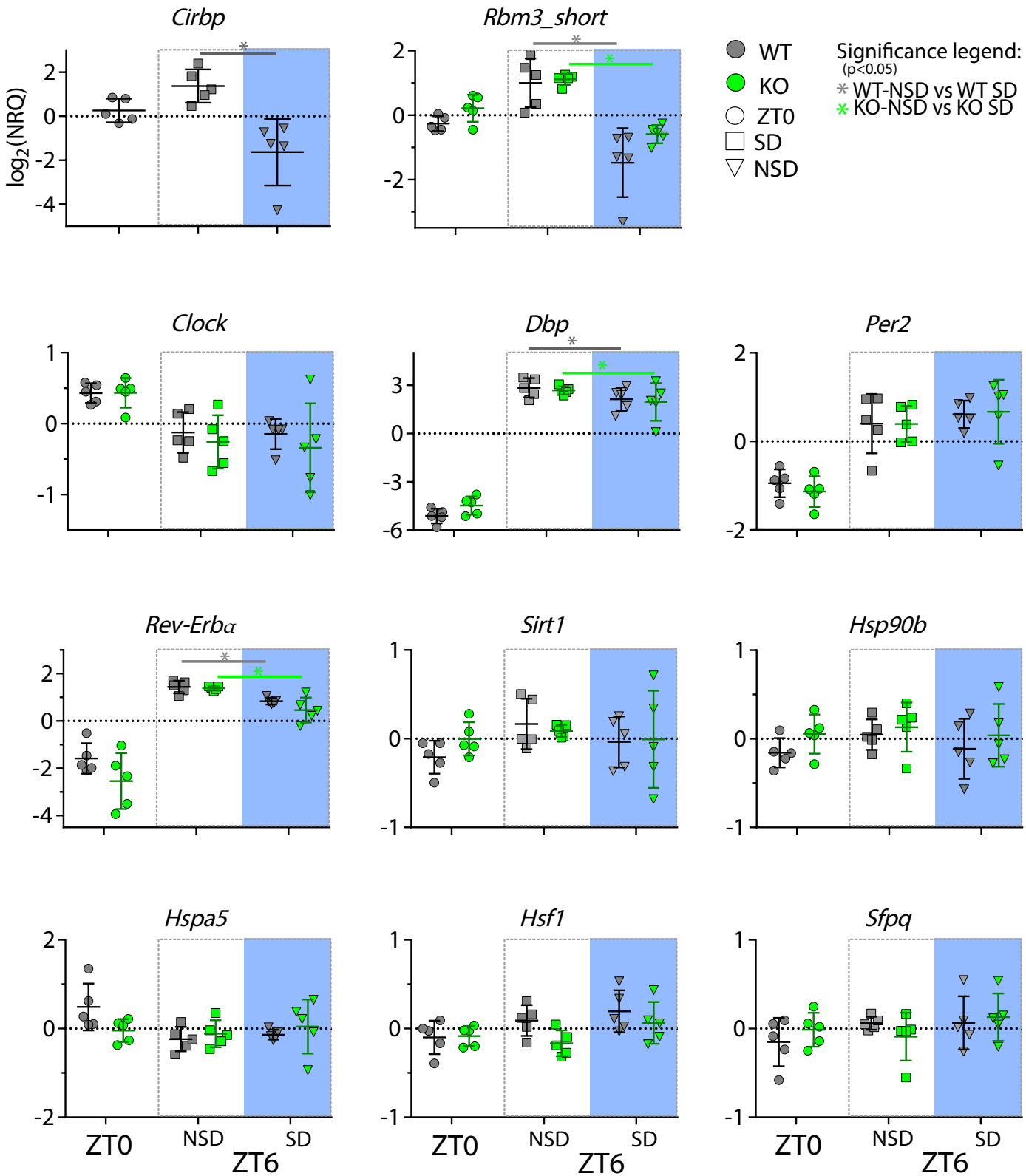
Cirbp
Rbm3_short
Clock
Dbp
Per2
Rev-Erbα
Sirt1
Hsp90b
Hspa5
Hsf1
Sfpq
log2(NRQ)
WT
KO
ZT0
SD
NSD
Significance legend:
(p<0.05)
WT-NSD vs WT SD
KO-NSD vs KO SD
ZT0
NSD
SD
ZT6

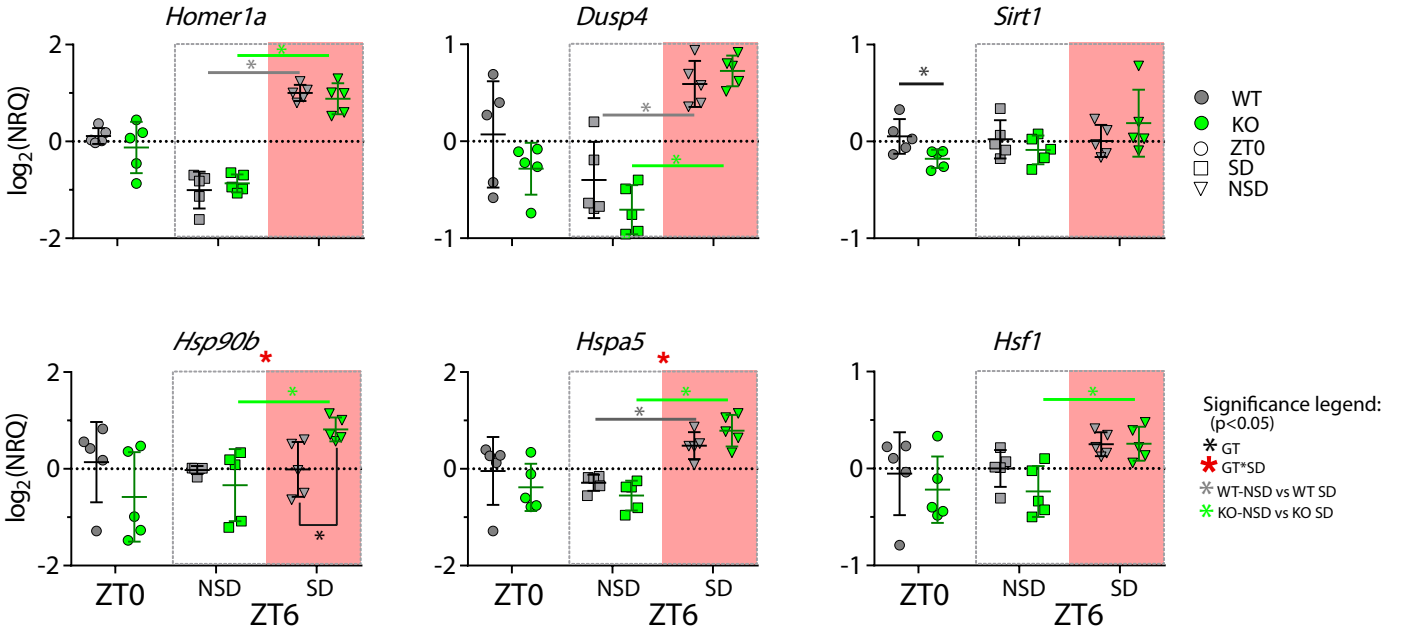
Homer1a
Dusp4
Sirt1
Hsp90b
Hspa5
Hsf1
log2(NRQ)
2
0
-2
1
-1
ZT0
NSD
SD
ZT6
WT
KO
ZT0
SD
NSD
Significance legend:
(p<0.05)
GT
GT*SD
WT-NSD vs WT SD
KO-NSD vs KO SD

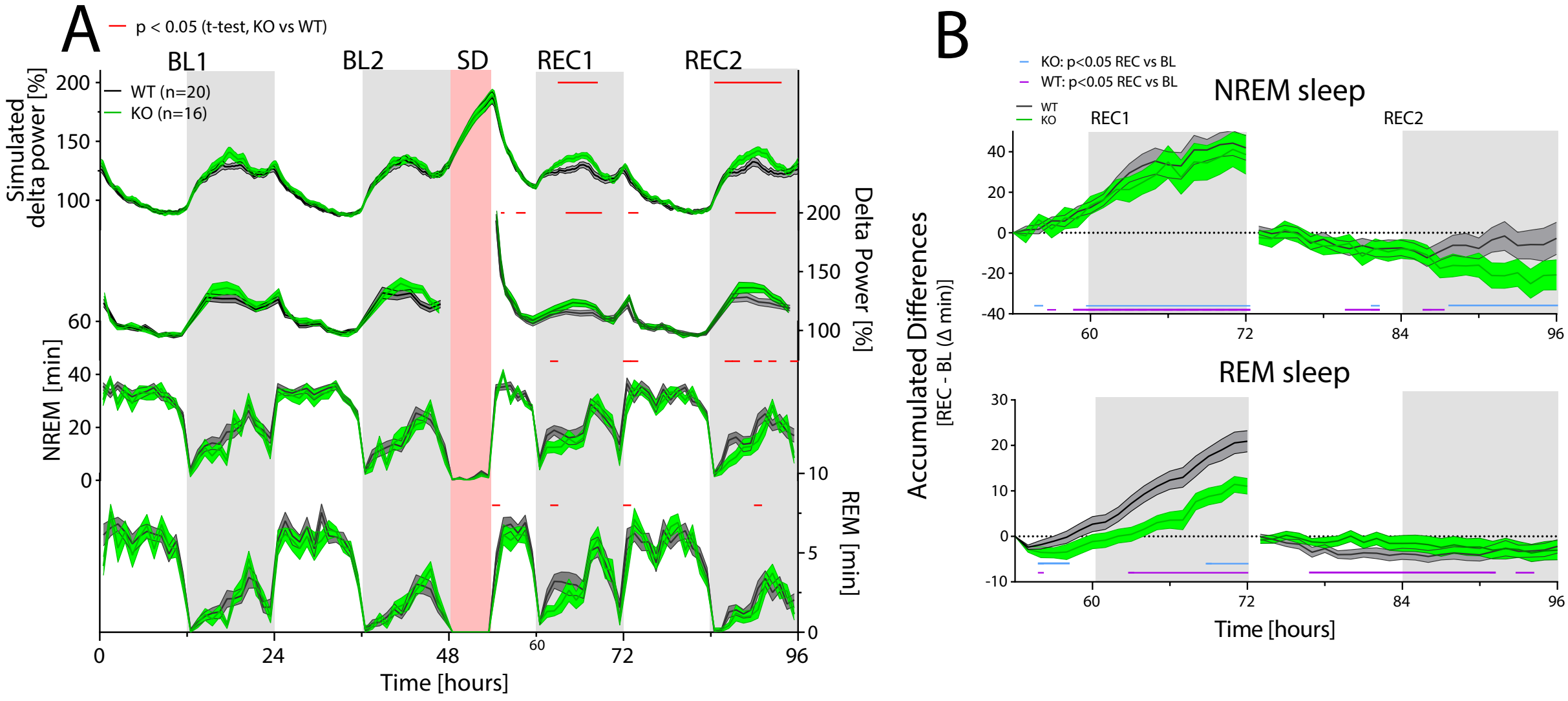
A
p < 0.05 (t-test, KO vs WT)
BL1
BL2
SD
REC1
REC2
WT (n=20)
KO (n=16)
Simulated delta power [%]
Delta Power [%]
NREM [min]
REM [min]
Time [hours]
B
KO: p<0.05 REC vs BL
WT: p<0.05 REC vs BL
WT
KO
NREM sleep
REC1
REC2
REM sleep
Accumulated Differences
[REC - BL (Δ min)]
Time [hours]

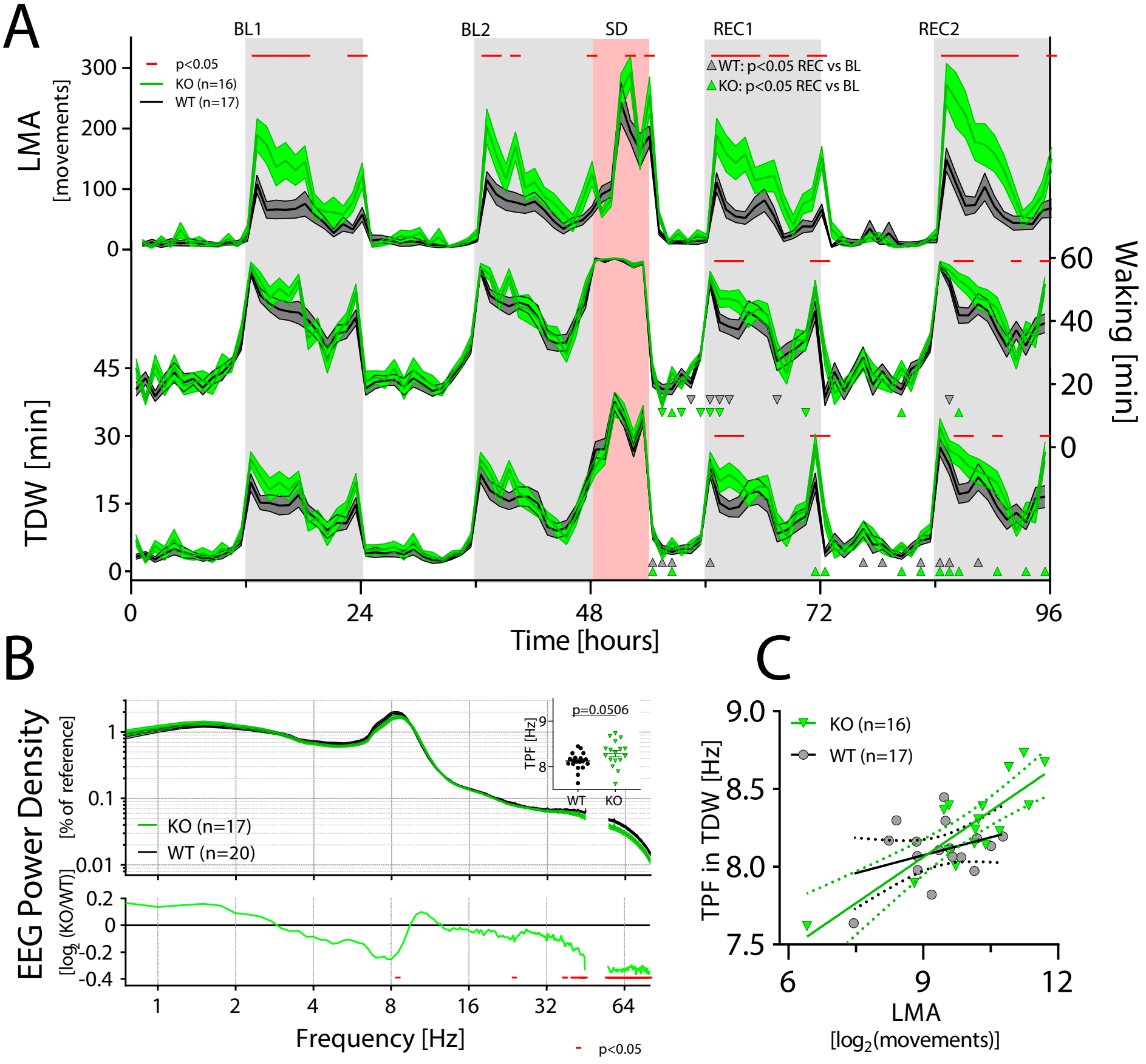
A
BL1
BL2
SD
REC1
REC2
p<0.05
KO (n=16)
WT (n=17)
WT: p<0.05 REC vs BL
KO: p<0.05 REC vs BL
LMA [movements]
TDW [min]
Waking [min]
Time [hours]
B
EEG Power Density [% of reference]
KO (n=17)
WT (n=20)
p=0.0506
TPF [Hz]
WT
KO
[log2 (KO/WT)]
Frequency [Hz]
p<0.05
C
KO (n=16)
WT (n=17)
TPF in TDW [Hz]
LMA [log2(movements)]

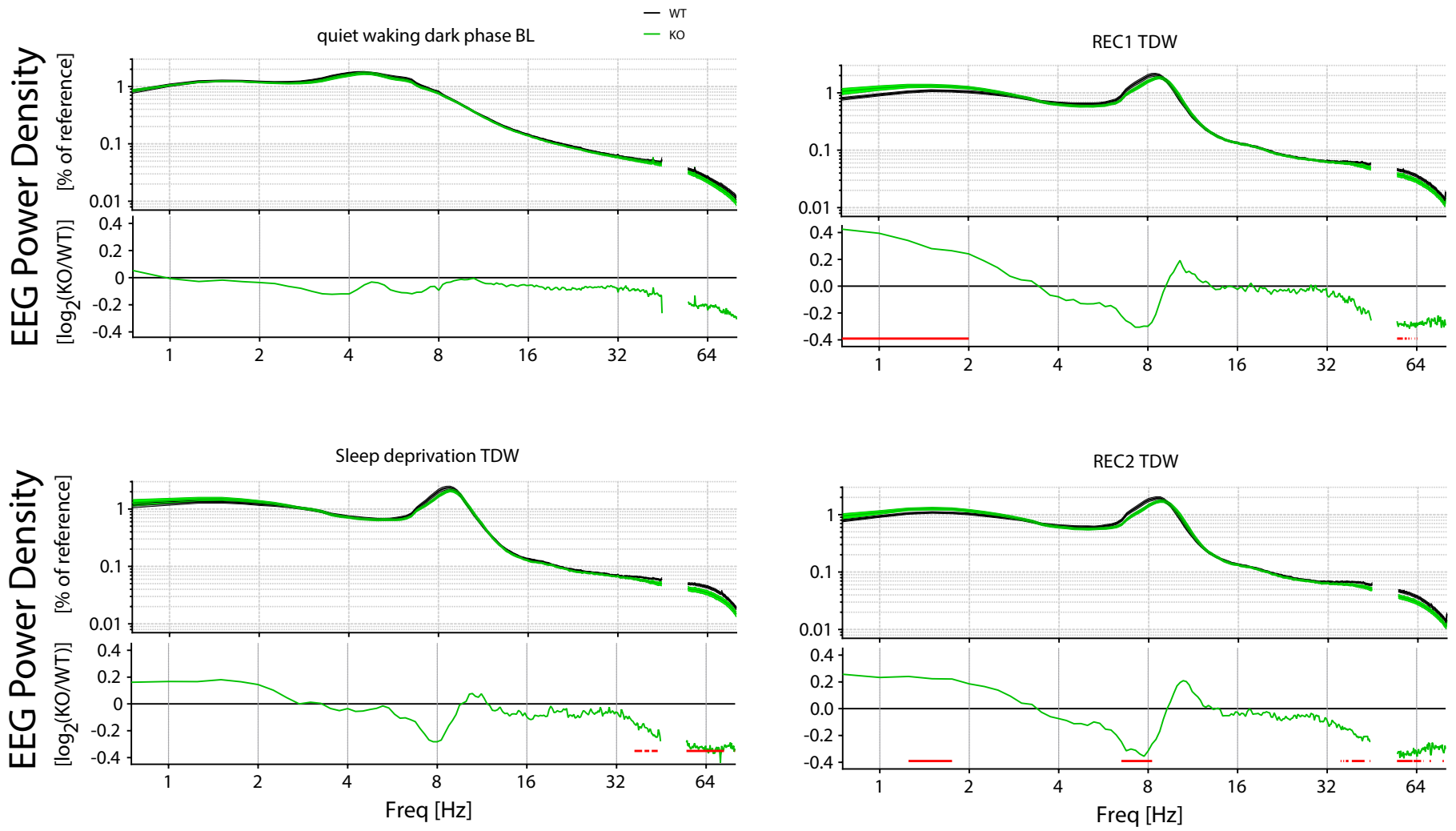
WT
KO
quiet waking dark phase BL
REC1 TDW
Sleep deprivation TDW
REC2 TDW
EEG Power Density
[% of reference]
[log2(KO/WT)]
1
0.1
0.01
0.4
0.2
0
-0.2
-0.4
0.0
1
2
4
8
16
32
64
Freq [Hz]

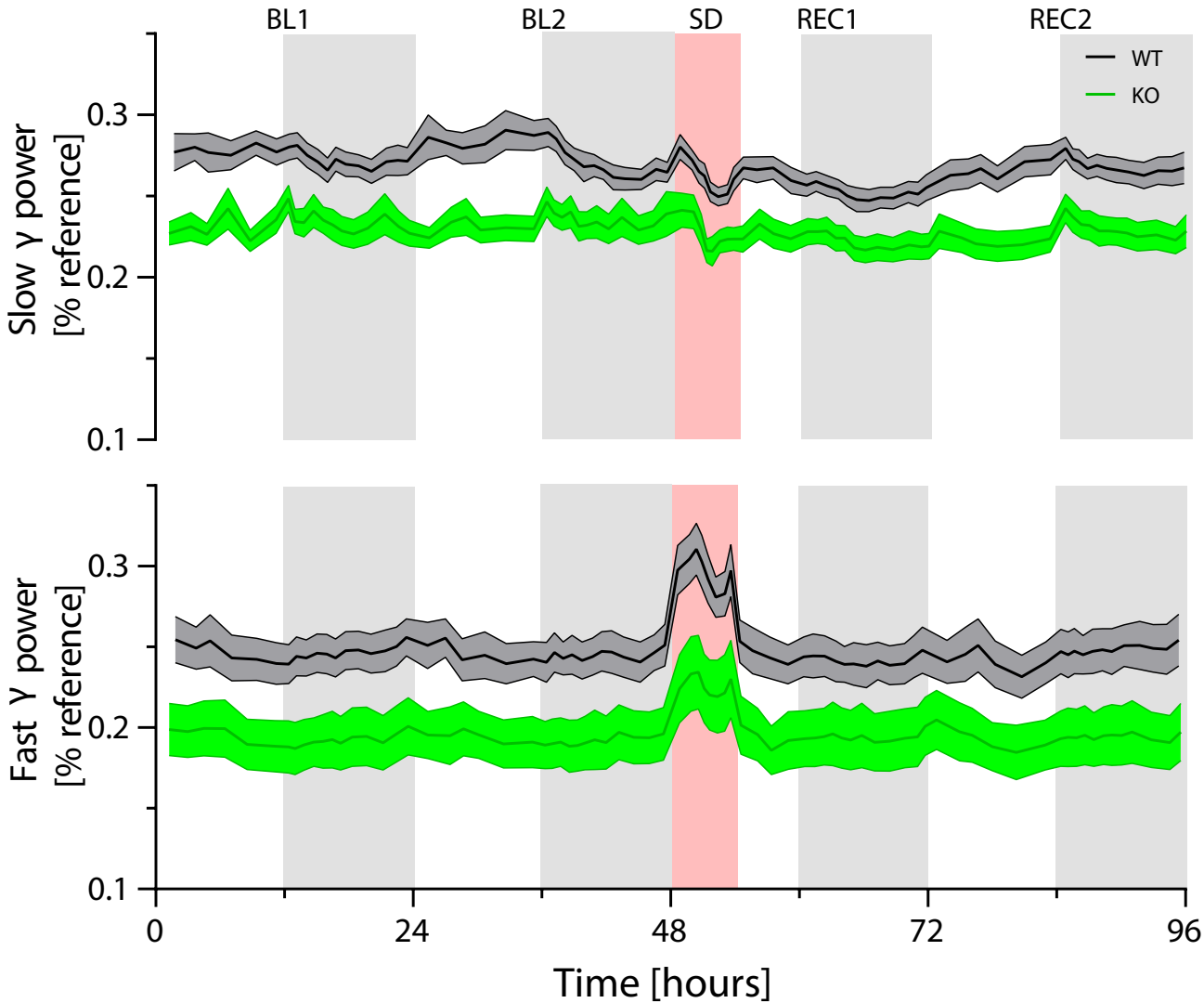
BL1
BL2
SD
REC1
REC2
WT
KO
Slow γ power
[% reference]
0.3
0.2
0.1
Fast γ power
[% reference]
0.3
0.2
0.1
0
24
48
72
96
Time [hours]

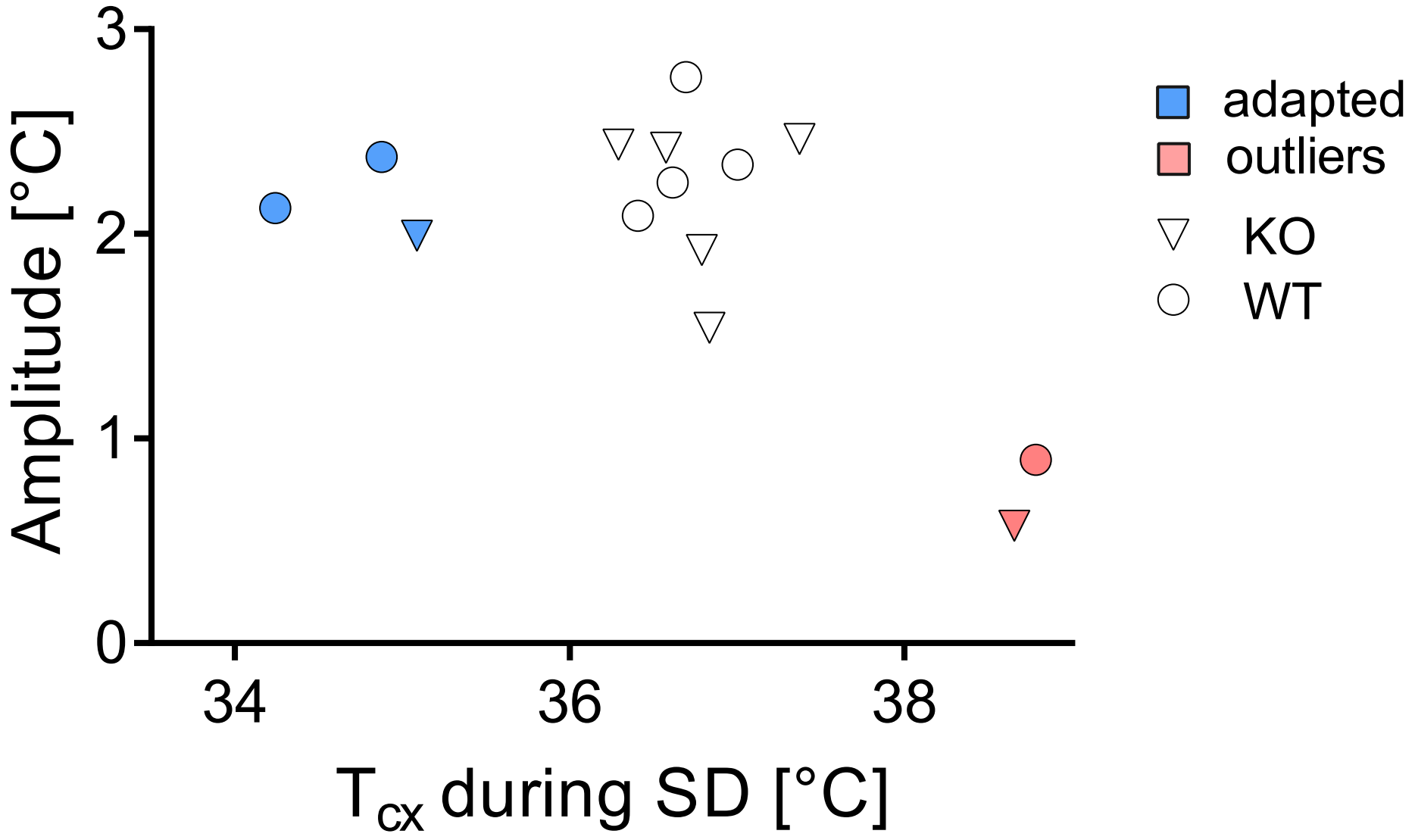
Amplitude [°C]
3
2
1
0
34
36
38
T_{cx} during SD [°C]
adapted
outliers
KO
WT